

UNCLASSIFIED

AD **436790**

DEFENSE DOCUMENTATION CENTER

FOR

SCIENTIFIC AND TECHNICAL INFORMATION

CAMERON STATION, ALEXANDRIA, VIRGINIA

19990302099



UNCLASSIFIED

NOTICE: When government or other drawings, specifications or other data are used for any purpose other than in connection with a definitely related government procurement operation, the U. S. Government thereby incurs no responsibility, nor any obligation whatsoever; and the fact that the Government may have formulated, furnished, or in any way supplied the said drawings, specifications, or other data is not to be regarded by implication or otherwise as in any manner licensing the holder or any other person or corporation, or conveying any rights or permission to manufacture, use or sell any patented invention that may in any way be related thereto.

64-12

FORWARDED BY:
CHIEF, BUREAU OF SHIPS TECHNICAL LIBRARY

436790

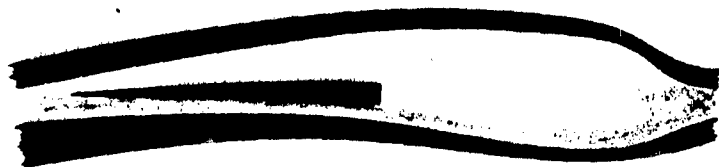
CATALOGED BY DDC

AS AD NO. _____

436790

Grumman

EXPERIMENTAL STUDY OF HIGH-SPEED HYDROFOILS



DDC
APR 28 1964
TL

QUALIFIED REQUESTERS MAY OBTAIN COPIES
OF THIS REPORT FROM DDC.

CONTRACT REQUIREMENTS	CONTRACT ITEM	MODEL	CONTRACT NO.	DATE
			84454	

REPORT

NO. XAR-A-45

DATE AUG. 26, 1963

EXPERIMENTAL STUDY OF
HIGH SPEED HYDROFOILS
VOLUME III

CODE 26512

H. R. Wright
PREPARED BY:

T. B. Street
CHECKED BY:

A. J. Wackand
APPROVED BY:

J. J. Wackand

REVISIONS

DATE	REV BY	REVISIONS & ADDED PAGES	REMARKS

ACKNOWLEDGMENT

This report is in fulfillment of the objectives set forth in Contract NObs 84454 sponsored by the Bureau Of Ships.

The cooperation and assistance in this program of Mr. Virgil E. Johnson, Jr. of Hydronautics, Inc. is acknowledged with gratitude.

TABLE OF CONTENTS

<u>Title</u>	<u>Page</u>
SUMMARY	1
INTRODUCTION	2
CONCLUSIONS	3
SYMBOLS	4
DISCUSSION	6
A. Model Description	6
B. Lift and Drag Prediction	7
C. Example	10
D. Correlations	11
REFERENCES	13
TABLES	14
FIGURES	18

SUMMARY

This test program was conducted to measure the hydrodynamic characteristics of a series of supercavitating and transcavitating hydrofoil models with various planforms and sections to provide a design procedure to predict hydrodynamic characteristics for this type hydrofoil. Twenty hydrofoil models were tested in the Grumman Whirling Tank at three depths and at a sufficient number of speeds and angles of attack to fully define their hydrodynamic characteristics. Lift, drag, pitching moment, and strut base pressure were measured for all models, and cavity pressure and foil base pressure were measured for the supercavitating models.

Classic supercavitating hydrofoil theory is shown to predict test results with an accuracy adequate for design if a modified value for the cross-flow lift coefficient is accepted.

INTRODUCTION

The work under this contract consisted of testing twenty supercavitating and transcavitating hydrofoil models in the Grumman Whirling Tank at three depths and at a sufficient number of speeds and angles of attack to fully define their hydrodynamic characteristics. The models include aspect ratios of 1.0 to 5.0, sweep angles of 0 to 56.3° , taper ratios of 0 to 1.00, design lift coefficients of 0 to .350, and were tested at cavitation numbers of .029 to .145.

Lift, drag, pitching moment, and strut base pressure were measured for all models, and cavity pressure and foil base pressure were measured for the supercavitating models. The foil cavity pressure was measured by means of a static pressure tap centrally located on the upper surface of one semi-span.

Analysis of the test results was limited to the fully ventilated lift and drag data; the transition from fully wetted to fully ventilated did not cover a significant angle of attack range on any foil tested. Transition from wetted to cavitating flow on these foils was characteristically accompanied by a very high frequency vibration audible as a loud screech. A study of this "singing" phenomenon did not conclusively identify the source but gave some indication that it was associated with a stall flutter type instability.

The work of this contract has been submitted in three volumes. Volume I presents the measured results in tabular form, the correlation of results, the structural analysis, and an analysis of the "singing" phenomenon encountered during the tests. Volume II presents the measured results in graphical form.

This volume summarizes the test results as a theory for the prediction of the lift and drag for a fully cavitating hydrofoil of arbitrary section and planform with a numerical example. Measured and predicted lift and drag are compared over ranges of submergence and hydrofoil geometric parameters as a measure of the reliability of the prediction procedure.

CONCLUSIONS

Classic ventilated hydrofoil theory provides adequate correlation for these results if a modified value for the cross-flow lift coefficient is accepted. With the modified cross-flow lift coefficient, the correlation of the fifty-nine measured lift and drag curves with classic ventilated hydrofoil theory may be summarized statistically as a prediction reliability (+ error indicates measurement higher than predicted):

	<u>Mean Error</u>	<u>Probable Error</u>
Lift Coefficient	-.002	<u>+.012</u>
Drag Coefficient	+.0012	<u>+.0028</u>

SYMBOLS

NOTE: All Dimensions in Ft./#/Sec./Radians Unless Otherwise Noted.

- A Aspect Ratio.
- A_n Section Coefficient. See Eqs. 2 and 3.
- A_o' Section Coefficient. See Eq. 1.
- b Span.
- c Chord.
- \bar{c} Chord in Transformed Plane = \sqrt{c} .
- C_D Total Foil Drag = $C_{D_v} + C_f$.
- C_f Schoenherr Drag Coefficient.
- C_{DL} Drag Coefficient Due to Lift. See Eq. 12.
- C_L Lift Coefficient.
- C_{L1} Lift Coefficient Due to Camber, Angle of Attack, and Cavitation Number. See Eq. 9.
- C_{Lc} Lift Coefficient Due to Crossflow. See Eq. 9.
- C_l Section Lift Coefficient.
- $C_{l\alpha}$ Section Lift Curve Slope. See Fig. 2.
- C_{l1} Design Section Lift Coefficient.
- ΔC_l Lift Coefficient Due to Cavitation Number. See Fig. 3.
- d Submergence.
- E Jones Edge Correction Factor. See Eq. 10.
- K_b Biplane Factor For Surface Effect. See Fig. 5.
- t Section Thickness.
- x Distance From Leading Edge.
- \bar{x} x in Transformed Plane = \sqrt{x}
- y Section Lower Surface Ordinate.
- \bar{y} y in Transformed Plane.
- α Foil Angle of Attack.
- α_o Camber Equivalent Angle of Attack, See Eq. 6 and Fig. 1.
- α_1 Induced Angle of Attack. See Eq. 11.
- $\alpha_o \tan^{-1} \left(\frac{-y'}{c} \right)$ T.E. - A_o'
- α_s Section Angle of Attack = $\alpha + A_o' + \alpha_c - \alpha_1$.
- γ Half-Angle Subtended by Circular Arc Section.
- θ Parameter Defining Distance Along Chord. See Eq. 5.

- Δ Foil Sweep. For $c/4$ Line Unless Otherwise Specified.
- λ Taper Ratio.
- σ Cavitation Number.
- σ_c Cavitation Number Based on Cavity Pressure.
- r Planform Correction Factor. See Fig. 6.

SUBSCRIPTS

- $/$ Lower.
- T.E. Trailing Edge.
- ∞ At Infinite Submergence.

DISCUSSION

A. Model Description

The twenty models of this program are described in Table III and the sections employed are shown on Figure 28. Each foil, except number 7, is mounted on a single 15% thick, blunt base parabolic strut. Foil number 7 is mounted on a twin strut combination. All the foil models have a curvature of 51 inch radius added to their ordinates to account for the streamline curvature of the Whirling Tank. This curvature is tangent to the foil chord line at 25% of the mean geometric chord of each model.

A static pressure tap is located at the base of the strut, on the base of each foil, and on the upper surface of each foil. The upper surface pressure tap is located at the 80% chord station on the middle of one semi-span.

B. Lift and Drag Prediction

Classic supercavitating hydrofoil theory, as presented by Johnson in Reference 1, was the basis for the correlation of these results. A number of variations of the classic theory were applied to the data but correlation was adequate only when a modified cross-flow lift coefficient was employed. The applicable equations of Reference 1 are repeated in this section.

The section coefficients are defined by Equation (11) of Reference 1:

$$(1) A_0' = -\frac{1}{\pi} \int_0^\pi \frac{dy}{dx} d\theta$$

$$(2) A_1 = \frac{2}{\pi} \int_0^\pi \frac{dy}{dx} \cos \theta d\theta$$

$$(3) A_2 = \frac{2}{\pi} \int_0^\pi \frac{dy}{dx} \cos 2\theta d\theta$$

where it is noted from Equation (5) of Reference 1 that

$$(4) \left(\frac{dy}{dx} \right)_{\bar{x}} = \left(\frac{dy}{dx} \right)_x$$

where $\bar{x} = \sqrt{x}$

and by definition

$$(5) \theta = \cos^{-1} \left(1 - 2 \frac{\bar{x}}{c} \right)$$

Note that the section coefficients are poorly defined at the leading edge (e.g. the 1% chord station is at nearly 20% of the θ scale) and that these coefficients are not defined at all for sections of infinite slope such as parabolic sections or sections cambered on the $a = 1.0$ mean line. Note further, however, that parabolic thickness distributions do not contribute to section angle of attack; that is

$$A_0' + \alpha_{c_m} = A_0' + A_1 - \frac{A_2}{2} = 0$$

for parabolic thickness distribution.

Where a section presents any significant curvature near the leading edge, therefore, accuracy is improved by subtracting an arbitrary amount of parabolic thickness distribution from the section ordinates. In practice it has proven convenient to subtract that amount of parabolic thickness which provides a zero ordinate at the first specified chord station.

By definition, the angle-of-attack increase due to camber is given at infinite submergence by

$$(6) \alpha_{c_{\infty}} = A_1 - \frac{A_2}{2}$$

The free surface effect on the section camber, $\alpha_c / \alpha_{c_{\infty}}$, may be taken from Figure 11 of Reference 1 which is presented here as Figure 1 for convenience. The curve for the Tulin-Burkart section was employed in the correlations of this report.

The section lift curve slope, $C_{l_{\alpha}}$, is taken from Figure 2 of Reference 1 which is presented here as Figure 2 for convenience.

The increment in lift coefficient added for finite cavitation number is that of Equation (4), of Reference 2 for a flat plate which is graphically presented in Figures 3 and 6 of Reference 2 and in Figure 3 of this report. The Auslaender equation (Equation 18 of Reference 3)

$$(7) \Delta C_l = C_{l_{\sigma=0}} + \frac{\sigma^2(1 - \frac{\sigma}{2})}{4C_{l_{\sigma=0}}} \quad (d=\infty, \sigma < .4)$$

$$\text{where } \Delta C_l = C_{l_{\sigma}} - C_{l_{\sigma=0}}$$

is compared with the Wu equation at two angles of attack for infinite aspect ratio on Figure 4. The difference between the two equations is a function of submergence, angle of attack, and planform and it is difficult to generalize. The two equations differ significantly only at cavitation numbers greater than .10 and section angles of attack less than about 6° . This operating condition was poorly covered by the configurations tested but gave some indication that the Auslaender equation is preferable for this region.

The section lift is given by

$$(8) C_l = C_{l_{\alpha}} (\alpha + A'_0 + \alpha_c) + \Delta C_l$$

and the three-dimensional lift coefficient is given by

$$(9) C_L = C_{L_1} + C_{L_c}$$

where:

$$C_{L_1} = \frac{C_{f_\alpha} \cos \Lambda c/2}{E} \alpha_s + \Delta C_{f_\alpha}$$

$$C_{L_c} = \frac{2.4}{AE} (1+\sigma) \sin^2 \alpha_{cr} \cos \alpha'_{cr}$$

$$\alpha_s = \alpha + \Lambda'_0 + \alpha_c - \alpha_1$$

$$\alpha_{cr} = \alpha + \Lambda'_0 + \alpha_c + \alpha_0$$

$$\alpha'_{cr} = \alpha + \Lambda'_0 + \alpha_0$$

The constant, 2.4, in the cross-flow lift coefficient expression was established on Figure 5 by favoring the results obtained at the higher values of the cross-flow lift parameter, $(1+\sigma) \sin^2 \alpha_{cr} \cos \alpha'_{cr} / AE$. All the data obtained for cross-flow lift parameters greater than .02 are presented on Figure 5 though only representative results are presented for lower values of the parameter. Additional testing on an extended range of the cross-flow lift parameter would be desirable for further substantiation of this important constant.

The Jones edge correction factor, E, may be taken from Figure 6 for foils having unswept half-chord lines or, in the general case, is given by

$$(10) E = \frac{2\lambda}{A(1+\lambda)} + \frac{1}{2} \sqrt{1 + \left[\tan \Lambda + \frac{1-\lambda}{A(1+\lambda)} \right]^2} + \frac{1}{2} \sqrt{1 + \left[\tan \Lambda - \frac{3(1-\lambda)}{A(1+\lambda)} \right]^2}$$

The induced angle of attack is given by

$$(11) \alpha_1 = \frac{C_{L_1} K_b}{\pi A} (1 + \tau)$$

where the biplane factor, K_b , and the Glauert planform correction factor, τ , may be taken from Figures 7 and 8.

The drag due to lift is given by

$$(12) C_{D_L} = C_{L_1} \tan (\alpha + \Lambda'_0) + C_{L_c} \tan (\alpha + \Lambda'_0 + \alpha_0)$$

The Schoenherr line is included in this Volume as Figure 9. Note that only the lower surface is wetted on the supercavitating hydrofoil. A roughness allowance of .0004 is suggested for prototype foils.

C. Example

Geometry (Foil No. 4, Figures 10 and 11)

Aspect Ratio, $A = 3.0$
 Quarter-chord Sweep Angle, $\Lambda = 0$
 Taper Ratio, $\lambda = .5$
 Thickness Ratio, $t/c = .131$
 Section: Parent (These specifications, from Reference 4, are not used in the performance calculations and the symbols are not employed elsewhere in the report)
 Design Lift Coefficient, $C_{L1} = .170$
 Camber Index, $c_2 = .0875$
 Design Angle of Attack, $\delta = 2.5^\circ$
 Semi-parabolic thickness, $\tau = 0$
 Induced Curvature Correction, $f = .0099$
 Submergence, $d/c = 1.0$
 Cavitation Number, $\sigma = .066$

Section Coefficients

The section is shown on Figure 10.

The chordwise distributions for $\frac{dy}{dx}$ and $\frac{dy}{dx} \cos n\theta$ are computed in

Table I and plotted on Figures 12, 13 and 14. Integration on Figures 12, 13, and 14 yields

$$A_0' = 2.11^\circ$$

$$A_1 = 2.75^\circ$$

$$A_2 = -1.46^\circ$$

where it should be noted that these results differ from the computer evaluations employed in Volume I by .5% to 2.5%.

By definition:

$$\begin{aligned} \alpha_{c_w} &= A_1 - A_2/2 \\ &= 2.75^\circ + 1.46^\circ/2 \\ &= 3.48^\circ \end{aligned}$$

Foil Lift and Drag

The foil lift and drag curves are derived in Table II. The supporting derivations required are as follows (note that computer derived section coefficients are employed here):

$$\begin{aligned}\alpha_1^0 &= 57.3 \frac{C_{L_1} K_b}{\pi A} (1+\tau) \\ &= 57.3 \times \frac{1.16}{3\pi} = 1.027 C_{L_1} \\ &= 7.24 C_{L_1} \\ \alpha_0^0 &= \tan^{-1} \left(\frac{-y'}{C} \right)_{T.E.} - A'_0 \\ &= \tan^{-1} .0421 = 2.06^\circ \\ &= .35^\circ\end{aligned}$$

D. Correlations

The measured lift and drag data are compared with the predictions for each foil in Part III, Volume I. Figures 15 - 27 of this Volume make these comparisons between the members of foil families included among the twenty foils tested in order to illustrate the ability of the theory to predict the effect of individual foil parameters. The data for all these figures have been reduced to zero cavitation number for direct comparison. Strut drag and foil friction drag have been removed from the measured drags to reduce the results to drag due to lift.

Correlation with aspect ratio (Figures 15 and 20) and camber (Figures 16 and 21) is good except for the foils of least camber which differ significantly in slope on Figure 16 and in position on Figure 21. The slope disagreement occurs frequently throughout the data but is not systematic with the hydrofoil configuration. Note that Foil No. 7 was excluded from Figure 20 because the struts failed before drag tares could be obtained.

The results for taper ratio effect (Figures 17 and 22) verify qualitatively that taper ratio becomes more significant as it approaches unity. The range of sweeps provided for the foils incorporating the parent section was too limited to present a significant sweep effect (Figures 18 and 23).

The taper ratio effect and the sweep effect (for small sweep angles) are both of the same order as the effect of the speed on the foil characteristics and further experience with this speed effect would be required to provide a data precision which would measure the effects of taper ratio and moderate sweep. The source for the

speed effect cannot be positively identified from the data. It is not a Froude Number effect because Froude Number is independent of speed in the Whirling tank. Observation of the flow about the Langley Model No. 5 in the water tunnel of Hydronautics, Inc. reveals persistent wetted flow in regions influenced by the strut and by the tip vortex and the data is consistent with lingering wetted flow followed by a more typical Reynolds Number effect.

The effect of submergence was negligible for all foils tested (Figures 19 and 24), the section lift curve slope effect being almost exactly offset by the camber effect.

Drag data throughout this report have been presented as polar drag curves because it is the foil lift/drag ratio which is of primary interest. For information, however, typical curves of drag vs. angle of attack are presented on Figures 25, 26, and 27. Figures 25 and 26 do not add anything to the interpretation of Figures 20 and 21, being virtual cross-plots of those figures. Figure 27 is presented as evidence that the poor correlation for Foil Nos. 16 and 17 of Figure 26 is not systematic with design lift coefficient.

REFERENCES

1. NACA NM L57E16, 1957, "Theoretical And Experimental Investigation of Arbitrary Aspect Ratio, Supercavitating Hydrofoils Operating Near The Free Water Surface", Virgil E. Johnson, Jr.
2. California Institute of Technology Report No. 47-4, 1955, "Comparison Of The Characteristics Of A Hydrofoil Under Cavitating And Non-cavitating Operation", T. Yao-Tsu Wu and Bryne Perry.
3. Hydronautics, Inc., Technical Report 001-7, 1962, "Low Drag Supercavitating Sections", Jakob Auslaender.
4. Hydronautics, Inc., Letter to Preliminary Design Branch, BuShips, 10 November 1960, "Section Ordinates of a Supercavitating Single Strut Wing Proposed for Experimental Investigation", Virgil E. Johnson, Jr.

TABLES

	<u>Page</u>
I. Section Coefficient Parameters	15
II. Predicted Foil Lift and Drag	16
III. Foil Geometry	17

SECTION COEFFIC

PARENT SECTION C₁

1	2	3	4	5	6	7	
$\frac{x}{c}$	$-\frac{y_1}{c}$	$\Delta \frac{x}{c}$	$-\Delta \frac{y}{c}$	$-\left(\frac{\partial \bar{y}}{\partial x}\right)_{\bar{x}}$	$\frac{\bar{x}}{c}$	$2 \frac{\bar{x}}{c}$	
0	0			(.008)	0	0	
.025	.0003	.050	.0004	.008	.1580	.3160	
.05	.0004	.050	.0004	.008	.2237	.4474	
.075	.0007	.050	.0004	.008	.2735	.5470	
.1	.0008	.075	.0006	.008	.3162	.6324	
.15	.0013	.100	.0009	.009	.7873	.7746	
.2	.0017	↑	.0010	.010	.4472	.8944	
.25	.0023		.0011	.011	.5000	1.000	
.3	.0028		.0013	.013	.5477	1.0954	-
.35	.0036		.0017	.017	.5920	1.184	-
.4	.0045		.0021	.021	.632	1.1264	-
.45	.0057		.0027	.027	.671	1.342	-
.5	.0072		.0033	.033	.707	1.414	-
.55	.0090		.0038	.038	.742	1.484	-
.6	.0110		.0048	.048	.775	1.550	-
.65	.0134		.0051	.051	.806	1.612	-
.7	.0161		.0058	.058	.837	1.674	-
.75	.0192		.0067	.067	.866	1.732	-
.8	.0228		.0077	.077	.894	1.788	-
.85	.0269		.0086	.086	.922	1.844	-
.9	.0314	↓	.0096	.096	.949	1.898	-
.95	.0365	.100	.0107	.107	.975	1.950	-
1.00	.0421			(.1245)	1.000	2.000	-

NOTE: Section is shown on Figure 10.

1, 2 Lower Surface Section Ordinates.

3, 4 Co-ordinate Differences

5 (4)/(3) Extrapolation for $x/c = 0$ & 1. See Figure 11.6 $\sqrt{(1)}$ 7 $2 \times (6)$ 

TABLE I

SECTION COEFFICIENT PARAMETERSPARENT SECTION $C_1 = .170$ $t/c = .131$
1

6	7	8	9	10	11	12	13	14
$\frac{x}{c}$	$2 \frac{x}{c}$	$\cos \theta$	θ°	θ	$\frac{dy}{dx}$ $x \cos \theta$	$2 \theta^\circ$	$\cos 2\theta$	$\frac{dy}{dx}$ $x \cos 2\theta$
0	0	1.000	0	0	-.00800	0	1	-.00800
.1580	.3160	.6740	46.9	.818	-.00538	93.8	-.0663	.00053
.2237	.4474	.5526	56.5	.986	-.00442	113.0	-.3905	.003125
.2735	.5470	.4530	63.1	1.102	-.00362	126.2	-.591	.004725
.3162	.6324	.3676	68.45	1.193	-.002935	136.9	-.730	.00584
.7873	.7746	.2254	77.0	1.343	-.00203	154.0	-.899	.00808
.4472	.8944	.1056	83.95	1.463	-.001056	167.9	-.979	.00979
.5000	1.000	0	90.0	1.57	0	180.0	-1.000	.01100
.5477	1.0954	-.0954	95.5	1.666	.00124	191.0	-.981	.01275
.5920	1.184	-.184	100.6	1.753	.00313	201.2	-.933	.01595
.632	1.1264	-.264	105.3	1.837	.00554	210.6	-.860	.01805
.671	1.342	-.342	110.0	1.920	.00923	220.0	-.766	.0207
.707	1.414	-.414	114.4	1.997	.01365	228.8	-.695	.0217
.742	1.484	-.484	118.85	2.07	.01840	237.7	-.534	.0203
.775	1.550	-.550	123.4	2.155	.0242	246.8	-.394	.01735
.806	1.612	-.612	127.6	2.255	.0312	255.2	-.2555	.01303
.837	1.674	-.674	132.3	2.31	.0391	264.6	-.0941	.00546
.866	1.732	-.732	137.0	2.39	.0490	274.0	.0698	-.00468
.894	1.788	-.788	142.0	2.48	.0607	284.0	.242	-.01863
.922	1.844	-.844	147.5	2.575	.0725	295.0	.423	-.0363
.949	1.898	-.898	153.8	2.68	.0862	307.6	.610	-.0586
.975	1.950	-.950	161.7	2.82	.1015	323.4	.803	-.0858
1.000	2.000	-1.000	180.0	3.14	.1245	360.0	1.000	-.1245

8 1-(7) 13 $\cos (12)$
 9 $\cos^{-1} (8)$ 14 $(5) \times (13)$
 10 $(9)/57.3$
 11 $(5) \times (8)$
 12 $2 \times (9)$



Figure 11.

PREDI

PARENT SECTION

FOIL NO. 1

1	2	3	4	5	6	7	8	9	10
α_s	$\frac{C_{1a}}{\text{DEG}}$	$C_{1e} = 0$	$\frac{C_{1e=0}}{E}$	ΔC_1	C_{L1}	α_1 DEG	$\alpha_1 - \alpha'_0 - \alpha_c$ DEG	α DEG	$\alpha_1 + \alpha_0$ DEG
8	.0305	.244	.188	.020	.208	1.51	-3.51	4.49	1.86
12	.0281	.337	.262	↓	.282	2.04	-2.98	9.02	2.39
16	.0260	.416	.321	↓	.341	2.47	-2.55	13.45	2.82
20	.0236	.472	.363	↓	.383	2.77	-2.25	17.75	3.12

1. Arbitrary 11.
2. Figure 2 12.
3. (1) x (2) 13.
4. .775 x (3) 14.
(c/2 Sweep is Neglected)
5. Figure 3 15.
6. (4) + (5) 16.
7. 7.27 x (6) 17.
8. From Figure 1, $\frac{\alpha_c}{\alpha_{c_m}} = .84$ 18.
- $\alpha_c = .84 \times 3.53 = 2.96^\circ$ 19.
- (8) = (7) - 2.06 - 2.96 20.
- (Computer Evaluations Employed) 21.
9. (1) + (8)
10. (7) + .35°



TABLE II

PREDICTED FOIL LIFT AND DRAG

PARENT SECTION $C_{11} = .170$ $d/c = 1.0$ $t/c = .131$ FOIL NO. 4 $A = 3.0$ $A = 0$ $\lambda = .5$

	9	10	11	12	13	14	15	16	17	18	19	20	21
$-\alpha_c$	α DEG	$\alpha_1 + \alpha_o$ DEG	α_{cr} DEG	α'_{cr} DEG	$\sin^2 \alpha_{cr}$ $\times \cos \alpha'_{cr}$	$C_{L_{cr}}$	C_L	$\alpha + A'_o$ DEG	$\alpha + A'_o + \alpha_o$ DEG	C_{D_1}	$C_{D_{cr}}$	C_{D_L}	C_D
1	4.49	1.86	9.86	6.90	.0291	.019	.227	6.55	6.90	.0239	.0023	.0262	.0304
8	9.02	2.39	14.39	11.43	.0602	.040	.322	11.08	11.43	.0553	.0081	.0634	.0676
5	13.45	2.82	18.82	15.86	.1005	.066	.407	15.51	15.86	.0945	.0187	.1132	.1174
5	17.75	3.12	23.12	20.16	.1437	.095	.478	19.81	20.16	.1377	.0348	.1725	.1767

11. $(1) + (10)$

12. $(9) + A'_o + \alpha_o = (9) + 2.41$

13. $\sin^2 (11) \times \cos (12)$

14. $\frac{2.4}{AE} (1 + e) \sin^2 \alpha_{cr} \cos \alpha'_{cr} = .66 \times (13)$

15. $(6) + (14)$

16. $(9) + 2.06^\circ$

17. $(16) + .35^\circ$

18. $(6) \times \tan (16)$

19. $(14) \times \tan (17)$

20. $(18) + (19)$

21. $C_{D_L} + C_{D_f} = (20) + .0042$



Foil Number	Aspect Ratio Λ	c/4 Sweep Angle-Deg. Λ	Taper Ratio λ	Thickness Ratio t/c	Design Lift Coeff. C_{L1}	Foil Section	Non
							d/c =
1	3.0	0	1.00	.118	0	Wedge	.048
2	3.0	0	1.00	.117	.275	Tulin	-
3	3.0	0	.30	.131	.170	Parent	.053
4	3.0	0	.50	.131	.170	Parent	.050
5	3.0	0	1.00	.131	.170	Parent	.048
6	1.0	0	1.00	.131	.170	Parent	.084
7	5.0	0	1.00	.131	.170	Parent	.029
8	3.0	10.0	.30	.131	.170	Parent	.051
9	3.0	20.0	.30	.131	.170	Parent	.051
10	2.0	56.3	0	.030	0	Flat	.076
11	2.0	24.2	.25	.030	0	Flat	.077
12	3.0	45.0	0	.030	0	Flat	.068
13	3.0	16.7	.25	.030	0	Flat	.051
14	3.0	45.0	0	.060	.200	Parabolic	.068
15	3.0	16.7	.25	.060	.200	Parabolic	.051
16	3.0	0	.50	.071	.059	Parent	.044
17	3.0	0	.50	.103	.117	Parent	.044
18	3.0	0	.50	.158	.230	Parent	.044
19	3.0	0	.50	.180	.287	Parent	.038
20	3.0	0	.50	.203	.350	Parent	.038

1

TABLE III
FOIL GEOMETRY

Foil Section	Nominal Cavitation No. σ_c			Velocity Range Knots	Angle of Attack Range	Comments
	d/c = .75	d/c = 1.00	d/c = 1.25			
Wedge	.048	.063	.078	40 - 80	0° to 10°	Model failed at 70 knots
Tulin	-	.088	.110	40 - 70	1° to 12°	
Parent	.053	.069	.085	40 - 80	-1.5° to 3°	
Parent	.050	.066	.081	40 - 80	-2° to 7°	
Parent	.048	.064	.078	40 - 80	-1° to 9°	Mounting screw failure at 70 Twin strut model - failed at 80 knots.
Parent	.084	.110	.145	40 - 70	-1° to 11°	
Parent	.029	.039	.048	40 - 70	-2° to 7°	
Parent	.053	.069	.085	40 - 80	-2° to 8°	
Parent	.053	.069	.085	40 - 80	-2° to 8°	Model failed at 45 knots Model failed at 80 knots
Flat	.076	.097	.121	40 - 45	-1° to 12°	
Flat	.077	.101	.125	40 - 80	-1° to 12°	
Flat	.062	.081	.101	40 - 80	-.5° to 9°	
Flat	.053	.071	.088	40 - 80	0° to 10°	
Parabolic	.063	.084	.103	40 - 80	-2° to 7°	
Parabolic	.053	.071	.088	40 - 80	-2° to 9°	
Parent	.049	.065	.079	40 - 80	-1° to 7°	
Parent	.049	.065	.079	40 - 96	-1° to 8°	
Parent	.049	.064	.080	40 - 95	-2° to 8°	
Parent	.039	.051	.063	40 - 96	-2.5° to 8°	
Parent	.039	.051	.062	40 - 95	-2° to 9°	



FIGURES

	Page
1. α_c vs. Submergence	20
2. Section Lift Curve Slope vs. Submergence	21
3. Cavitation Number Lift Increment	22
4. Lift Increment - Wu vs. Auslaender	23
5. Cross-flow Coefficient, C_{Lcr}	24
6. Jones Edge Correction Factor vs. Aspect Ratio	25
7. Biplane Factor, K_b	26
8. Planform Correction Factor, r	27
9. Friction Drag Coefficient	28
10. Parent Foil Section	29
11. Lower Surface Slope - Parent Section	30
12. dy/dx vs. θ - Parent Section	31
13. $dy/dx \cos \theta$ vs. θ - Parent Section	32
14. $dy/dx \cos 2\theta$ vs. θ - Parent Section	33
15. Lift Correlation - Aspect Ratio Effect	34
16. Lift Correlation - Camber Effect	35
17. Lift Correlation - Taper Ratio Effect	36
18. Lift Correlation - Sweep Effect	37
19. Lift Correlation - Submergence Effect	38
20. Lift Correlation - Aspect Ratio Effect	39
21. Drag Correlation - Camber Effect	40
22. Drag Correlation - Taper Ratio Effect	41

FIGURES (Cont'd.)

	Page
23. Drag Correlation - Sweep Effect	42
24. Drag Correlation - Submergence Effect	43
25. Drag Correlation vs. α - Aspect Ratio Effect	44
26. Drag Correlation vs. α - Camber Effect	45
27. Drag Correlation vs. α - Flat Foil	46
28. Foil and Strut Sections	47

FIGURE 1 EFFECTIVE ANGLE OF ATTACK DUE TO CAMBER, α_c vs. SUBMERGENCE
From Figure 11 of Ref. 1

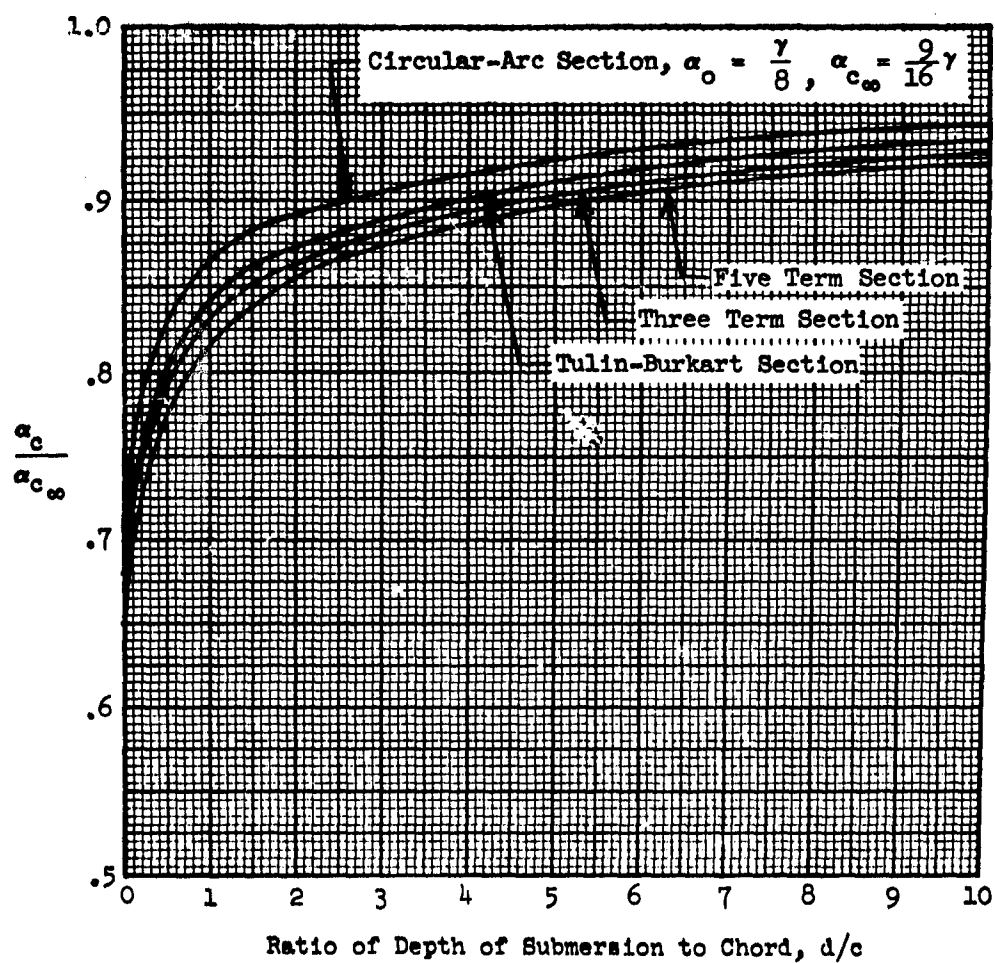


FIGURE 2 SECTION LIFT CURVE SLOPE VS. SUBMERGENCE
From Figure 2 of Ref. 1

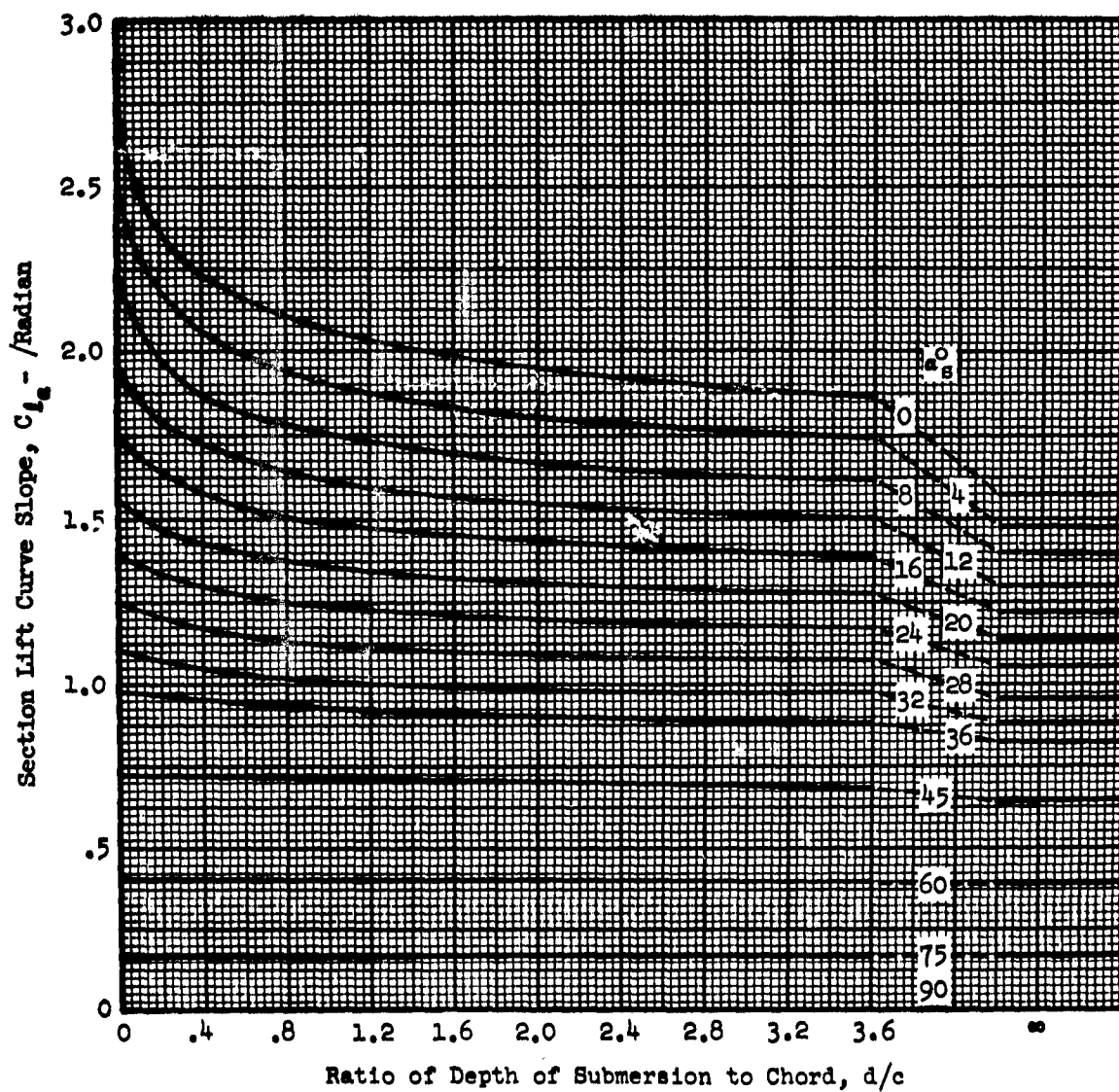


FIGURE 3 CAVITATION NUMBER LIFT INCREMENT
Flat Plate Infinite Submergence

Wu

Derived From Ref. 2

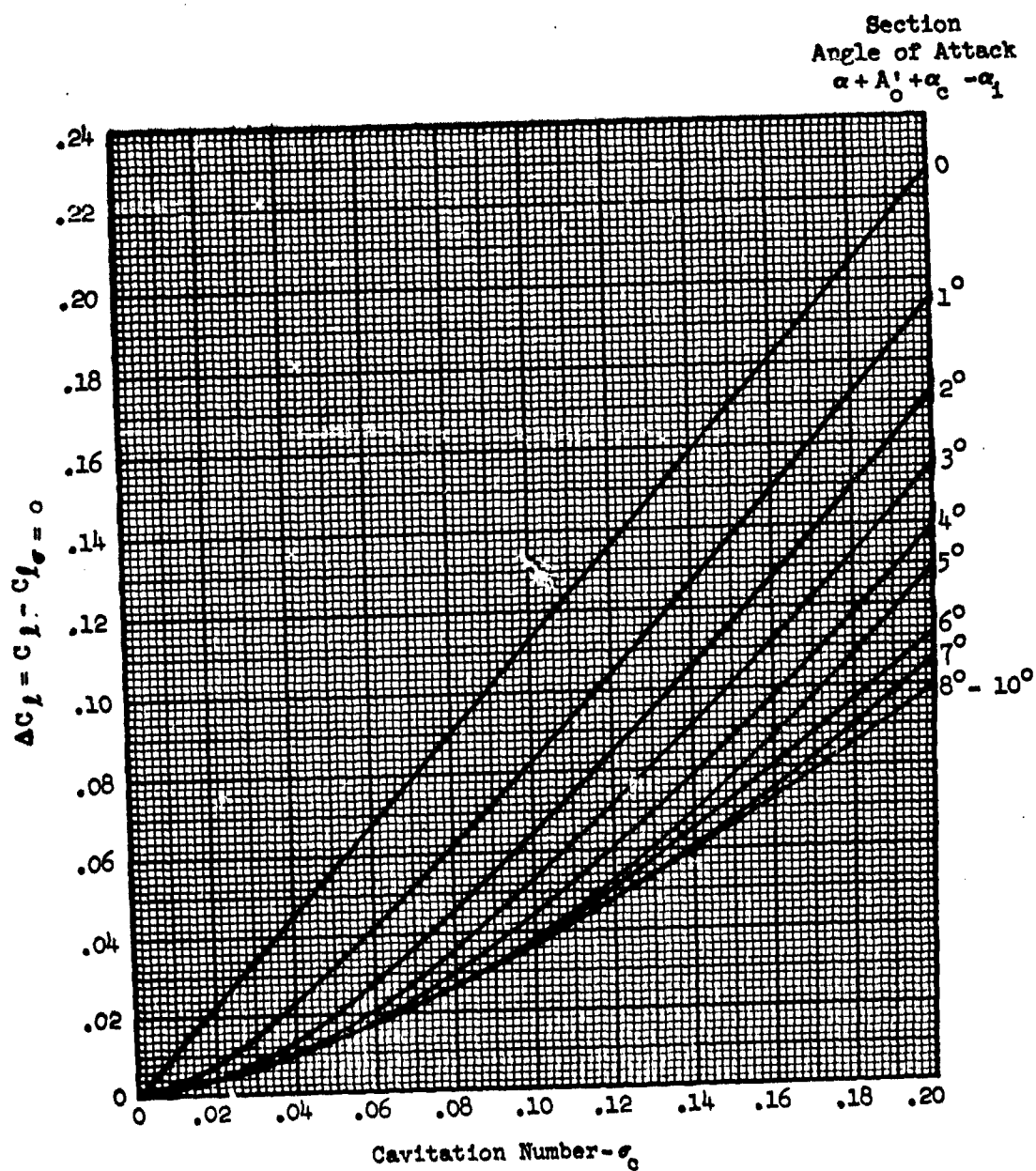


FIGURE 4 CAVITATION NUMBER LIFT INCREMENT-WU AND AUSLAENDER
Flat Plate- Infinite Aspect Ratio

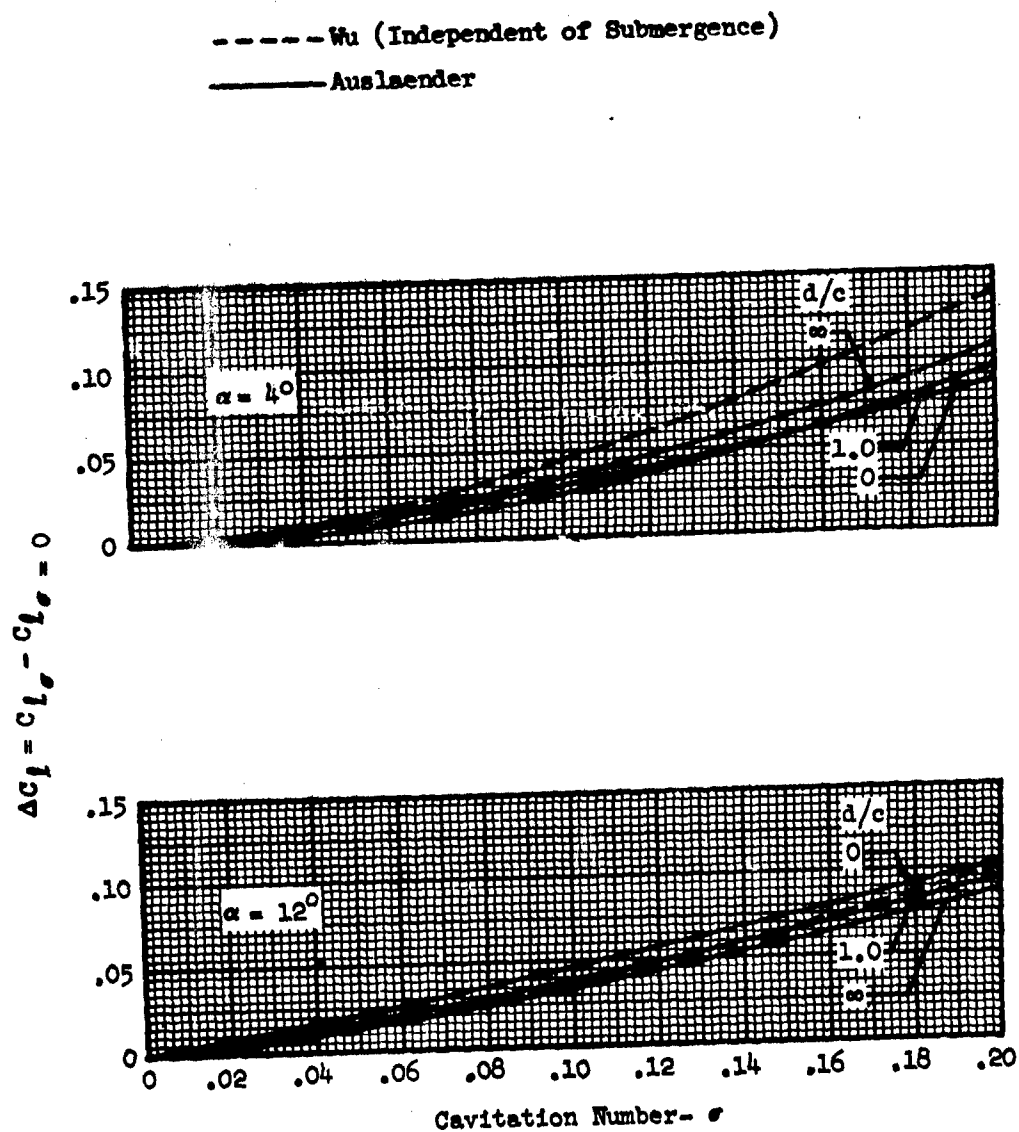


FIG. 5 CROSS-FLOW LIFT

$$\Lambda = 0$$

$$d/c = .75-1.25$$

	Foil	Section	C_{l_1}	Λ	λ	σ
○	1	Wedge	0	3	1.00	.048-.078
▽	2	Tulin	.275	3	1.00	.088-.110
▽	5	Parent	.170	3	1.00	.048-.078
◇	6	Parent	.170	1	1.00	.084-.145
□	7	Parent	.170	5	1.00	.029-.048
△	18	Parent	.230	3	.50	.049-.080
□	20	Parent	.350	3	.50	.039-.062

$$C_{L_C} = \frac{2.4}{AE} (1 + \sigma) \sin^2 \alpha_{cr} \cos \alpha'_{cr}$$

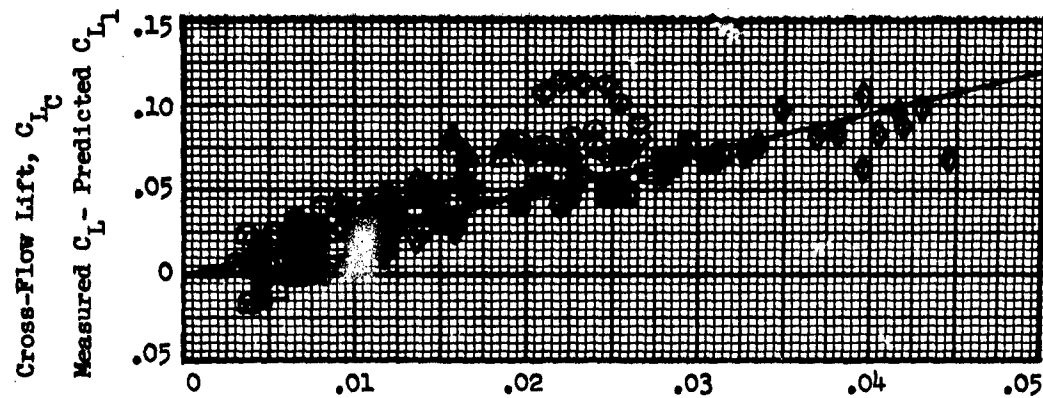


FIGURE 6 JONES EDGE CORRECTION FACTOR vs. ASPECT RATIO

$$E = \frac{\text{Semi-Perimeter}}{\text{Span}}$$

Unswept Half-Chord Line

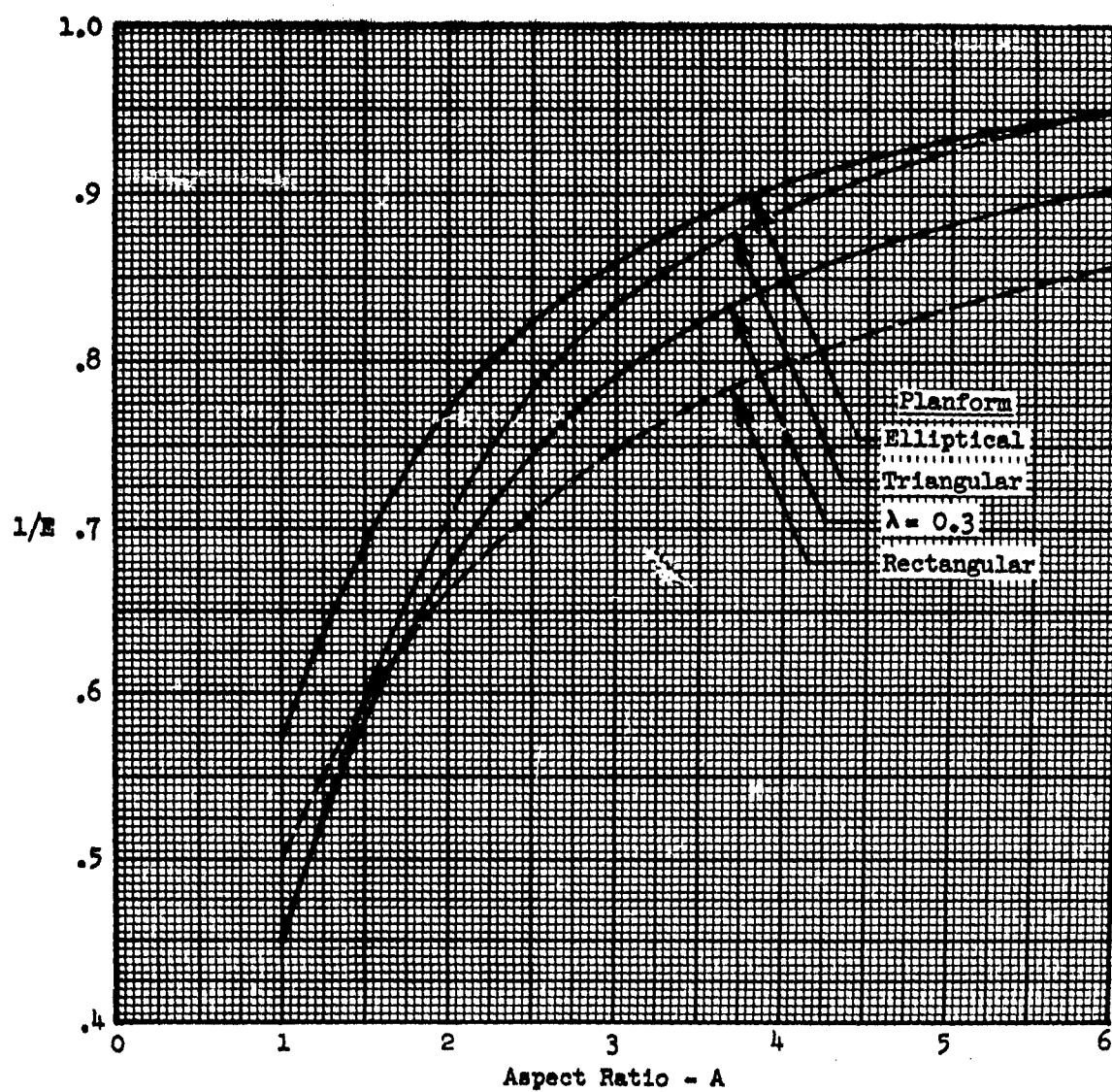


FIGURE 7 BIPLANE FACTOR, K_b

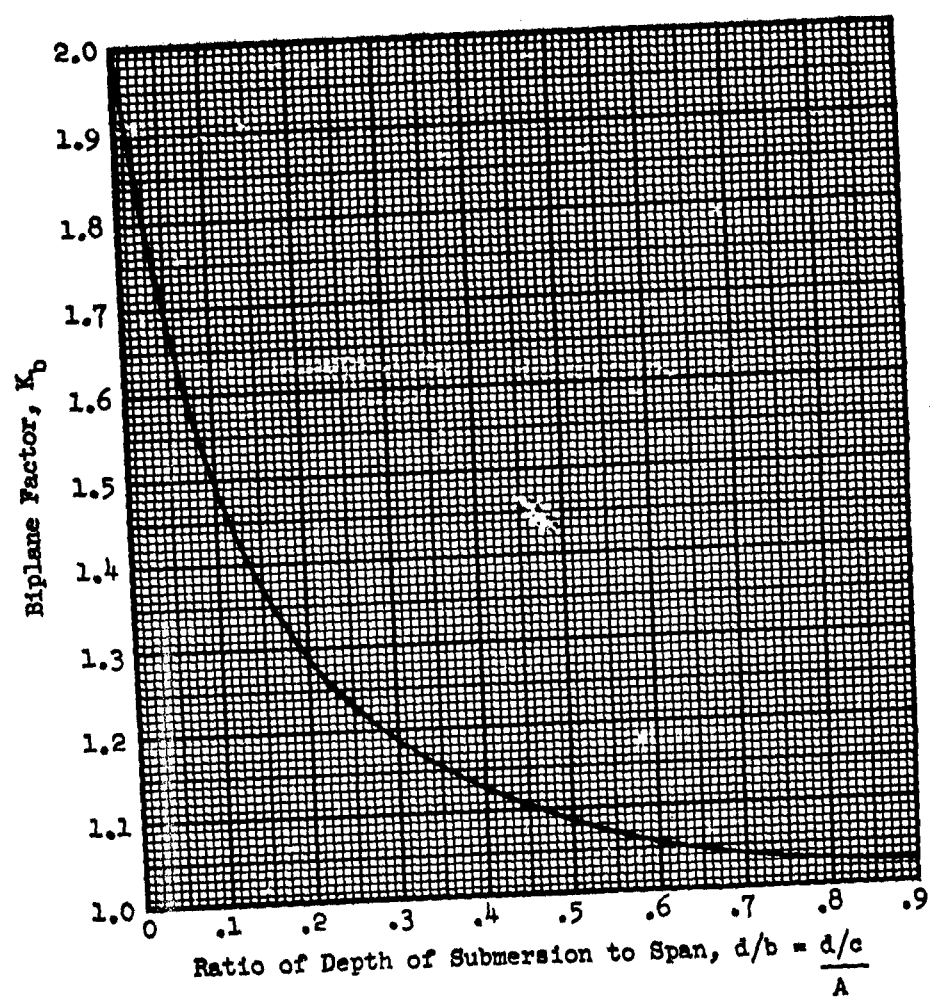


FIGURE 8 PLANFORM CORRECTION FACTOR, τ

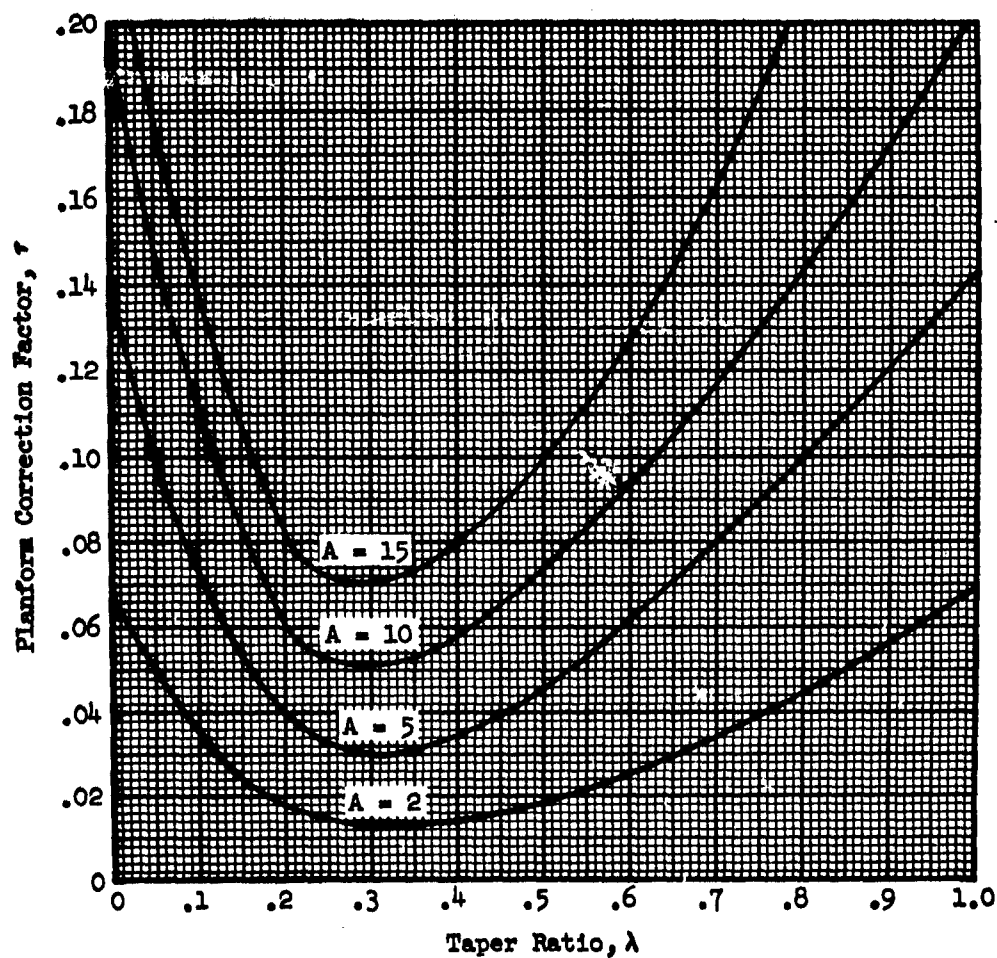


FIGURE 9 FRICTION DRAG COEFFICIENT vs. REYNOLDS NUMBER

C_f Based on Wetted Area

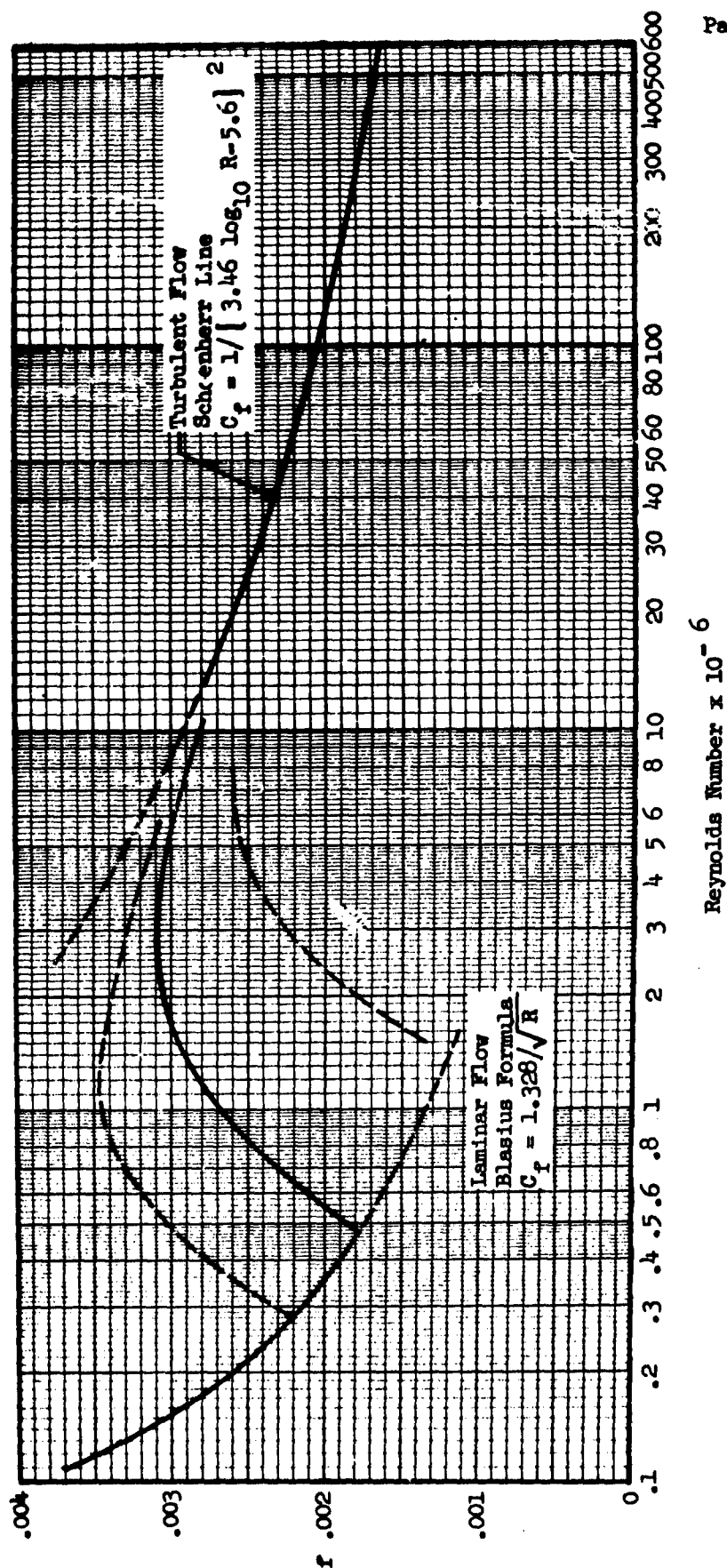


FIGURE 10 PARENT FOIL SECTION
Tulin-Burkart "Two Term" Section
Modified For One Chord Depth
 $Cl_1 = .170$ $t/c = .131$

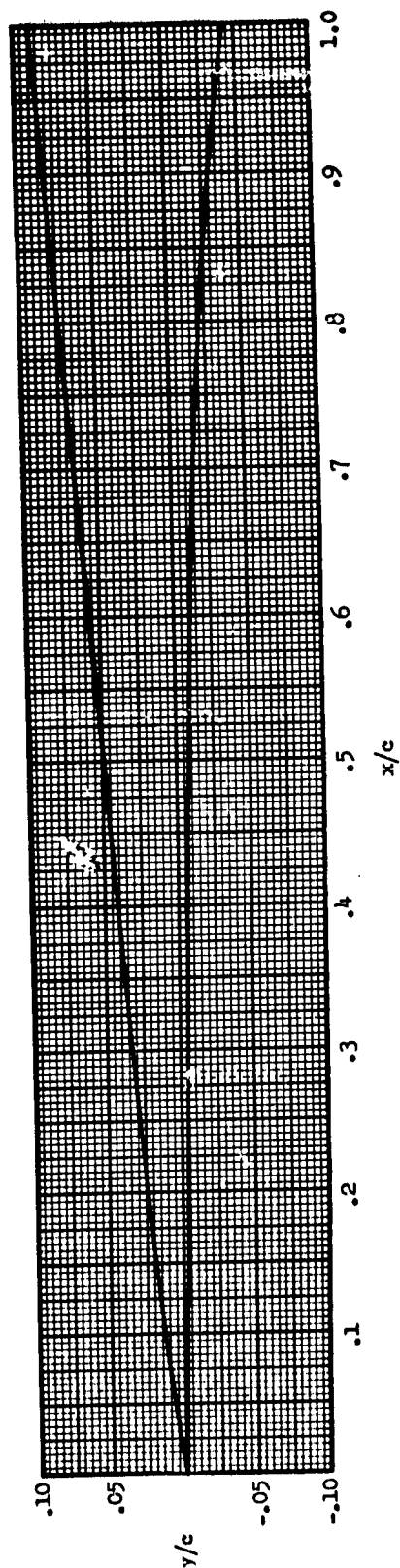


FIGURE 11 LOWER SURFACE SLOPE

Parent Foil Section

$$C_{l_1} = .170 \quad t/c = .131$$

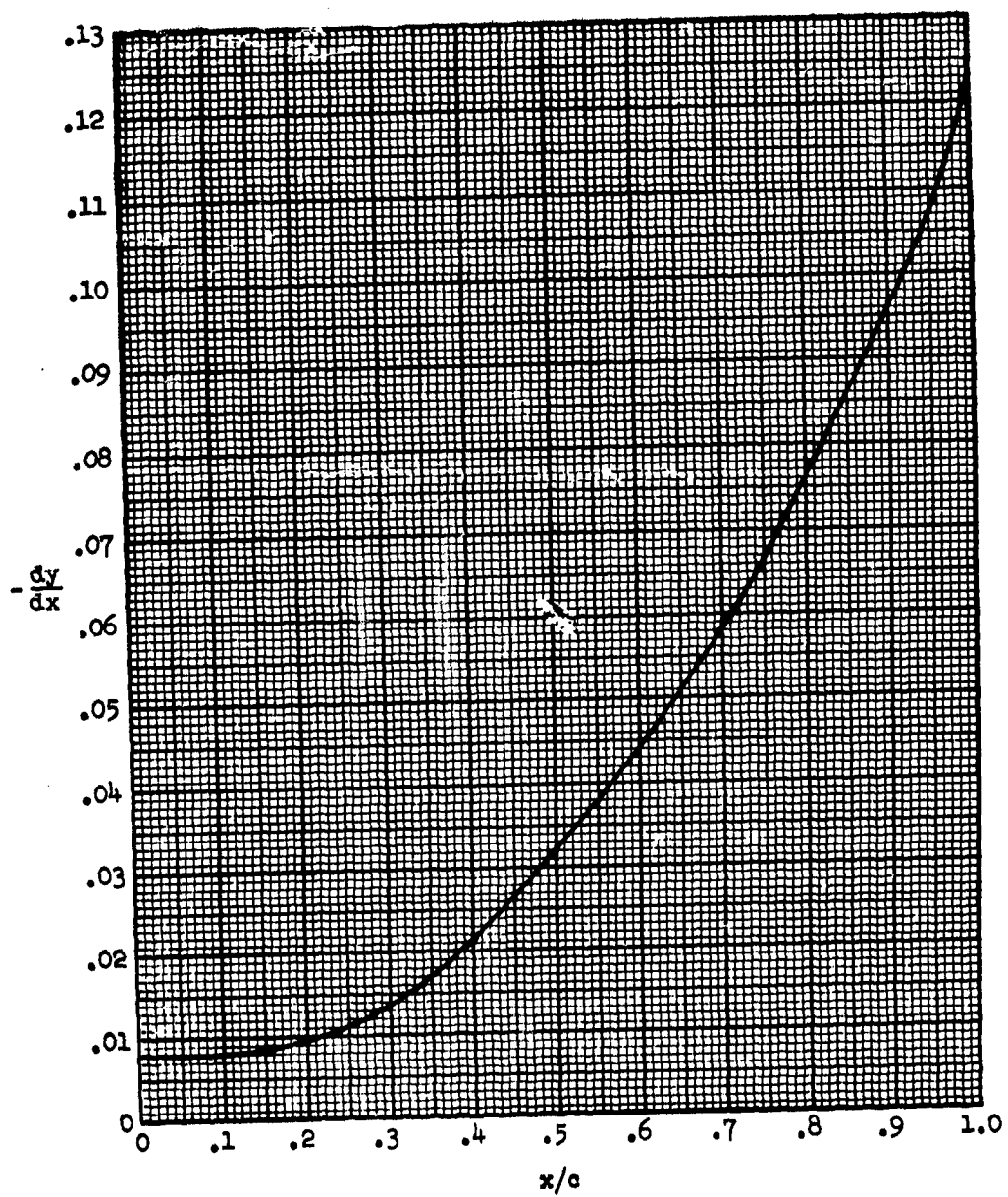


FIGURE 12 dy/dx vs. θ
 Parent Section
 $C_{L1} = .170$ $t/c = .131$

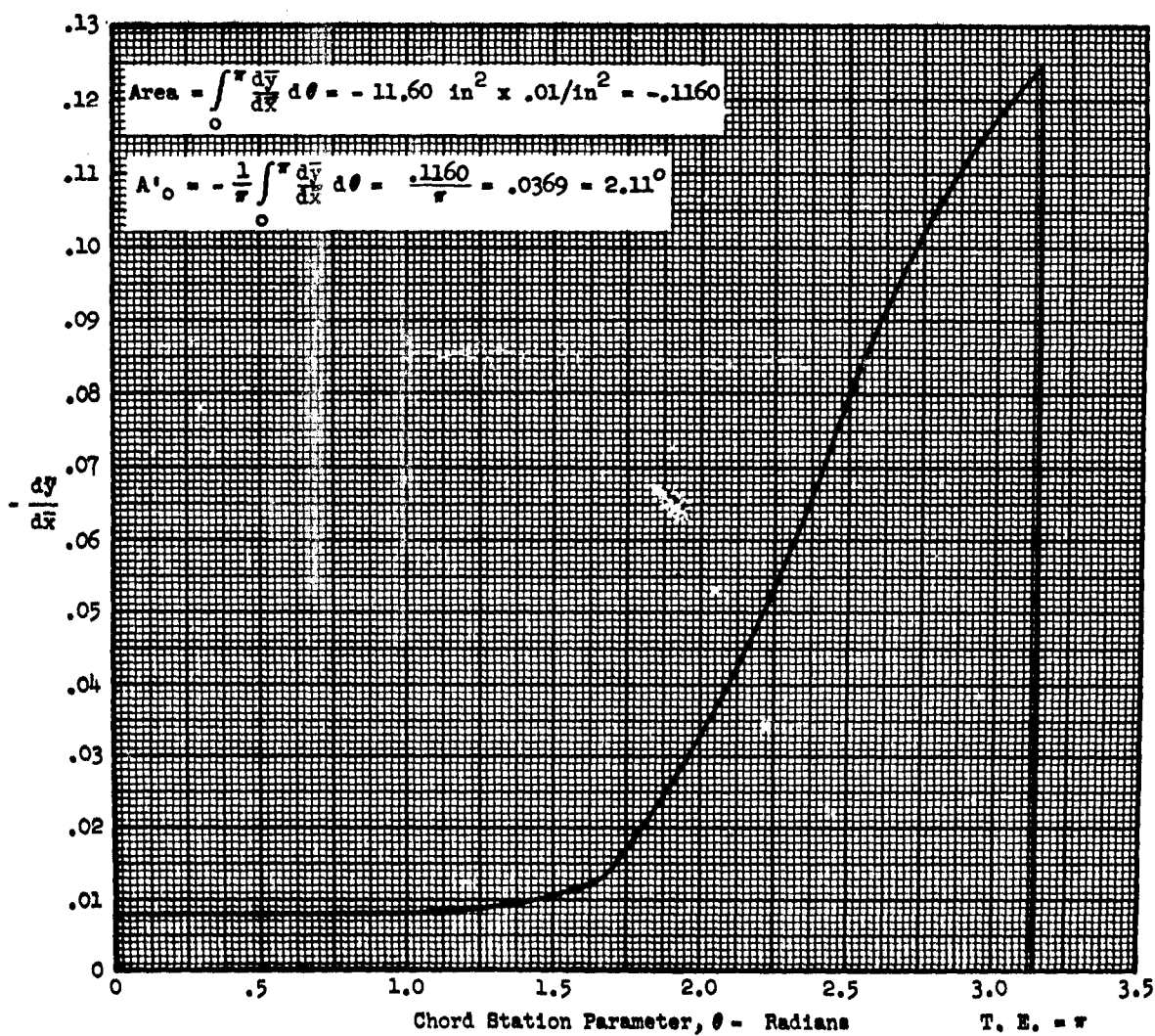


FIGURE 13 $\frac{dy}{dx} \cos \theta$ vs. θ

Parent Section

$$C_{l_1} = .170 \quad t/c = .131$$

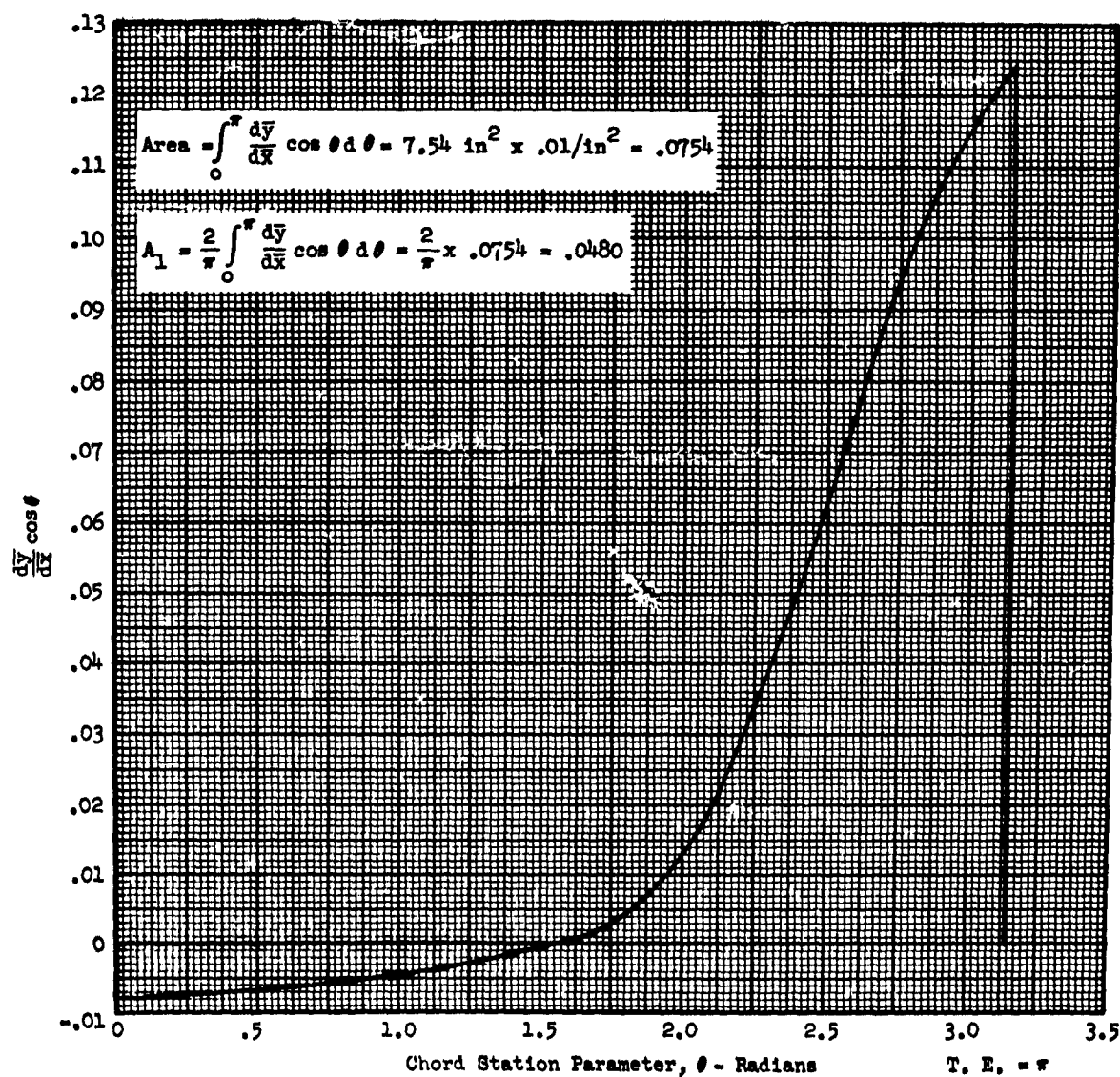


FIGURE 14 $\frac{dy}{dx} \cos 2\theta$ vs. θ

Parent Section

$$C_1 = .170 \quad t/c = .131$$

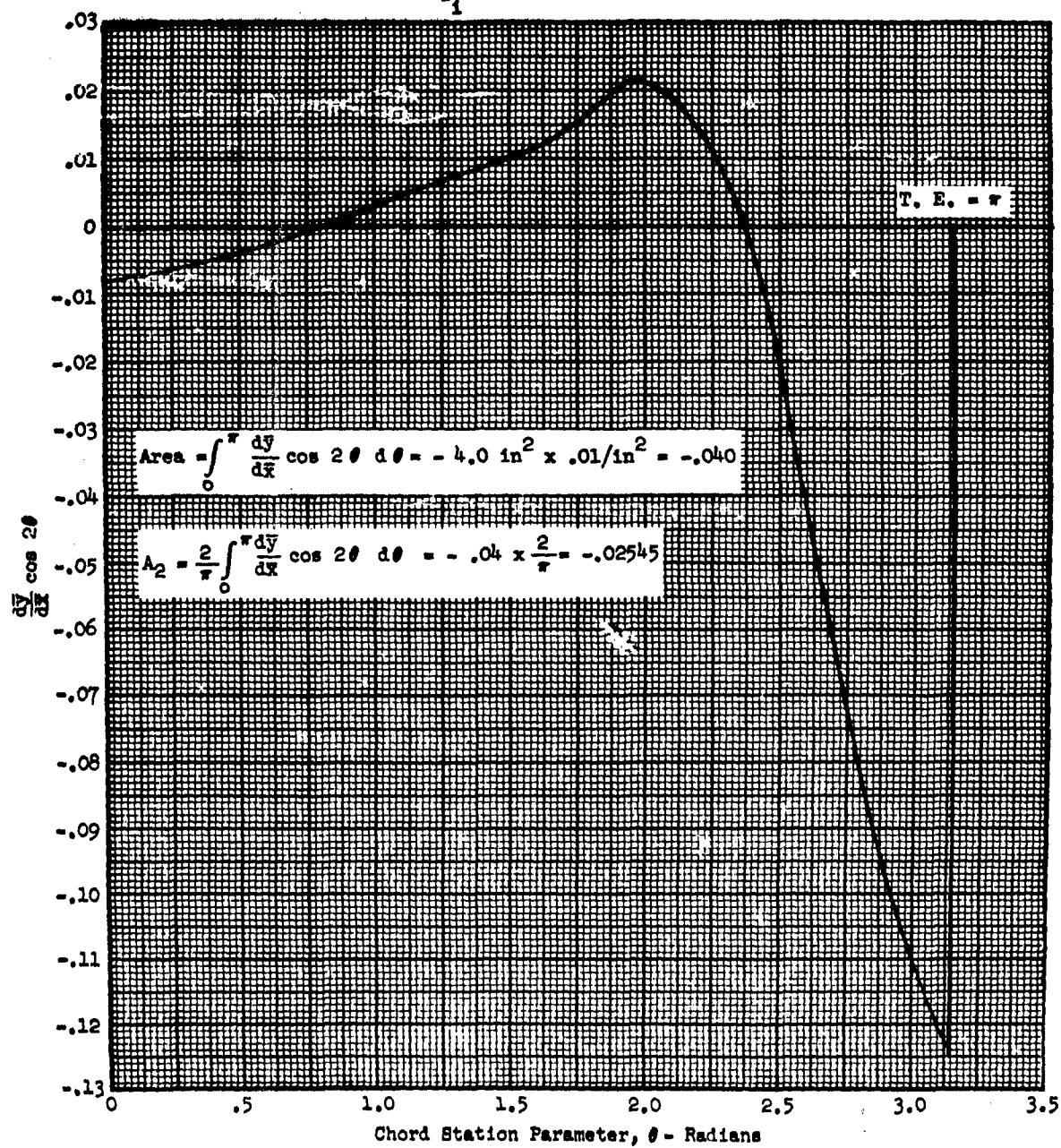


FIGURE 15 LIFT CORRELATION-ASPECT RATIO EFFECT
Parent Section - $C_{L1} = .170 - t/c = .131$

$\lambda = 1.0$

$A = 0$

$e = 0$

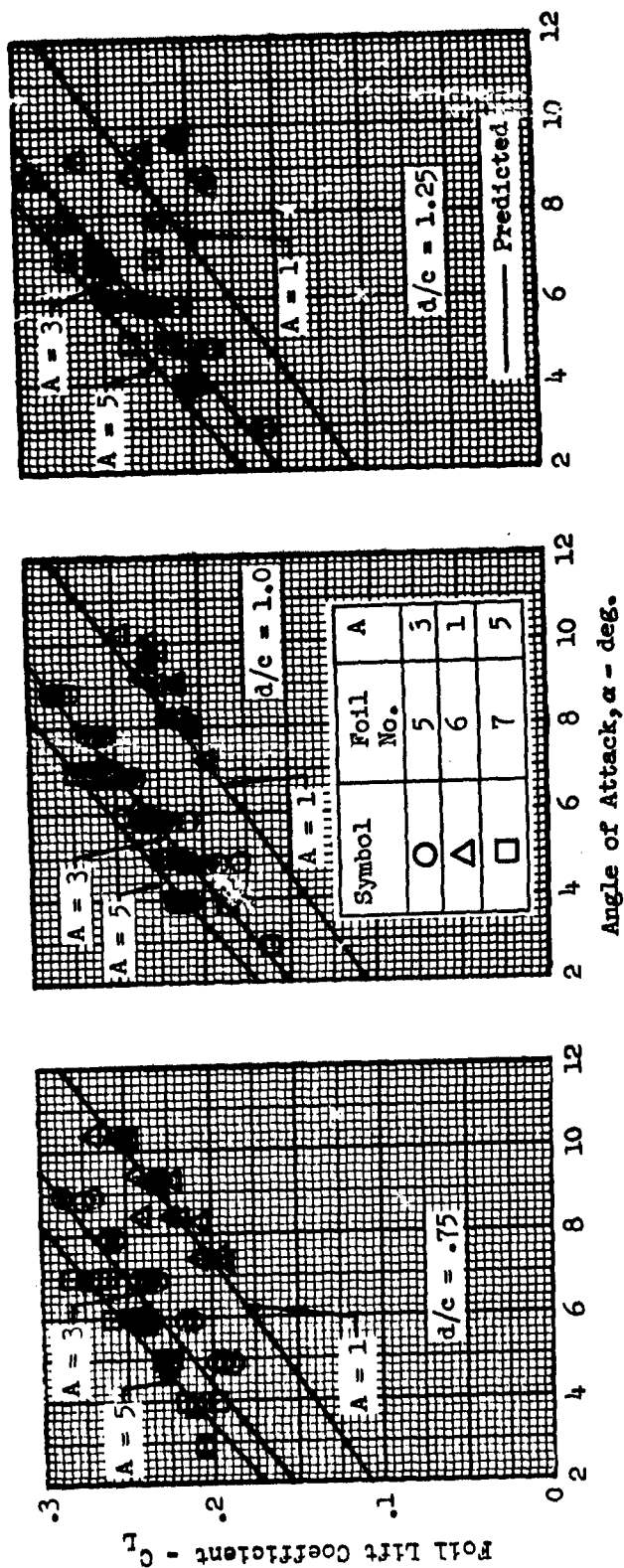


FIGURE 16 LIFT CORRELATION-CAMBER EFFECT

Parent Section

 $\Lambda = 3$ $\Lambda = 0$ $\lambda = .5$ $\sigma = 0$

— Predicted

Symbol	Foil No.	C_{l_1}	t/c	Nominal σ *		
				$d/c = .75$	$d/c = 1$	$d/c = 1.25$
□	4	.170	.131	.050	.066	.081
○	16	.059	.071	.049	.065	.079
△	17	.117	.103	.049	.065	.079
□	18	.230	.158	.049	.064	.080
◇	19	.287	.180	.039	.051	.063
◇	20	.350	.203	.039	.051	.062

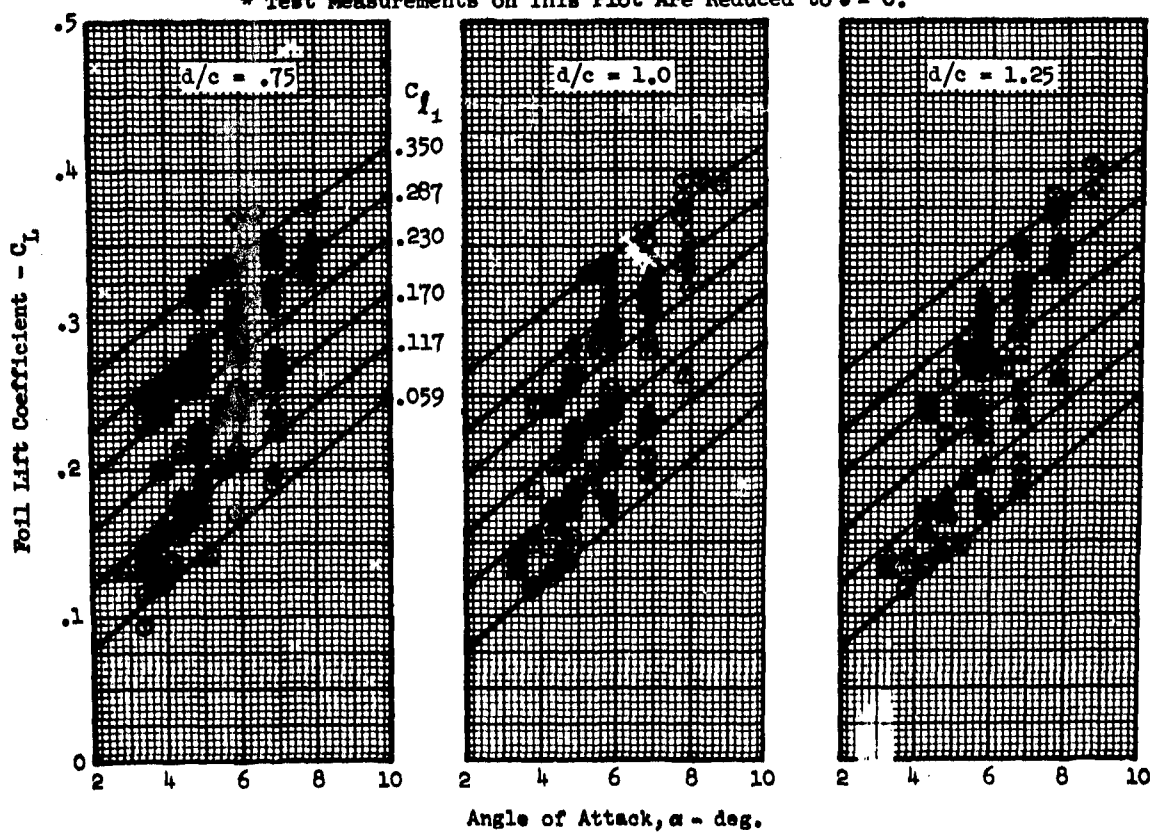
* Test Measurements on This Plot Are Reduced to $\sigma = 0$.

FIGURE 17 LIFT CORRELATION-TAPER RATIO EFFECT

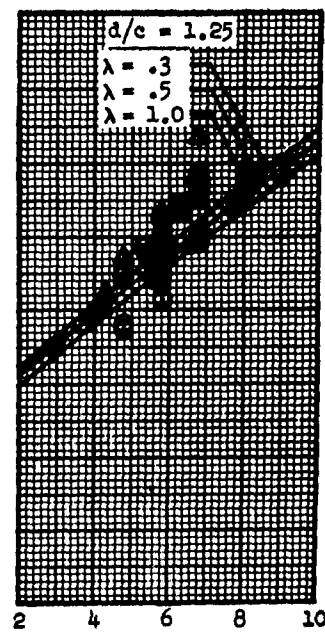
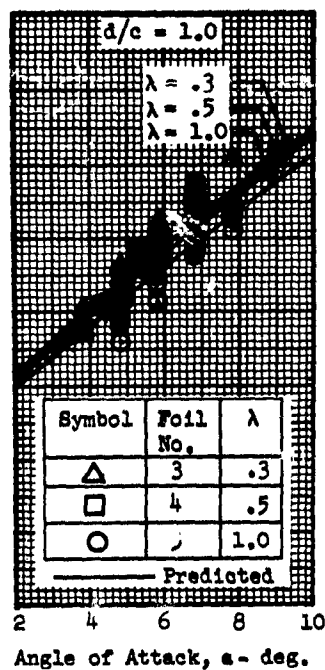
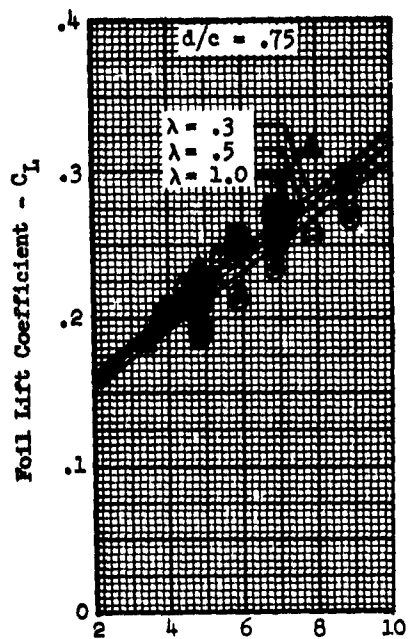
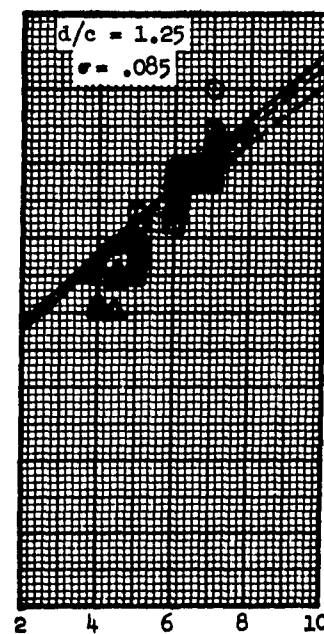
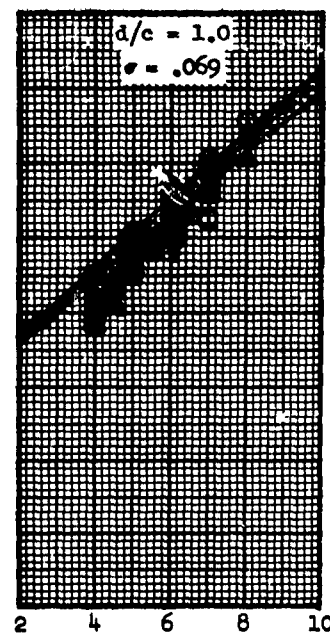
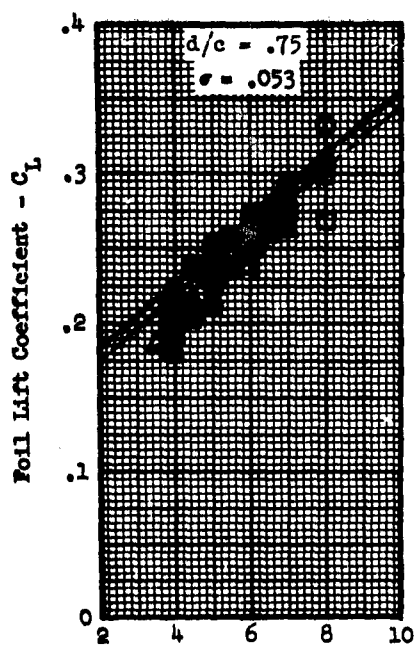
Parent Section - $C_{l_1} = .170$ - $t/c = .131$
 $\Lambda = 0$
 $\Lambda = 3.0$
 $\sigma = 0$


FIGURE 18 LIFT CORRELATION-SWEEP EFFECT
Parent Section - $C_{l_1} = .170$ - $t/c = .131$

$A = 3$

$\lambda = .3$

Prediction	Meas.	Foil No.	A
————	○	3	0°
-----	△	8	10°
-----	□	9	20°



Angle of Attack, α - deg.

FIGURE 19 LIFT CORRELATION-SUBMERGENCE EFFECT

Parent Section
 $\Lambda = 3$ $\Lambda = 0$ $\lambda = .5$
 $\sigma = 0$

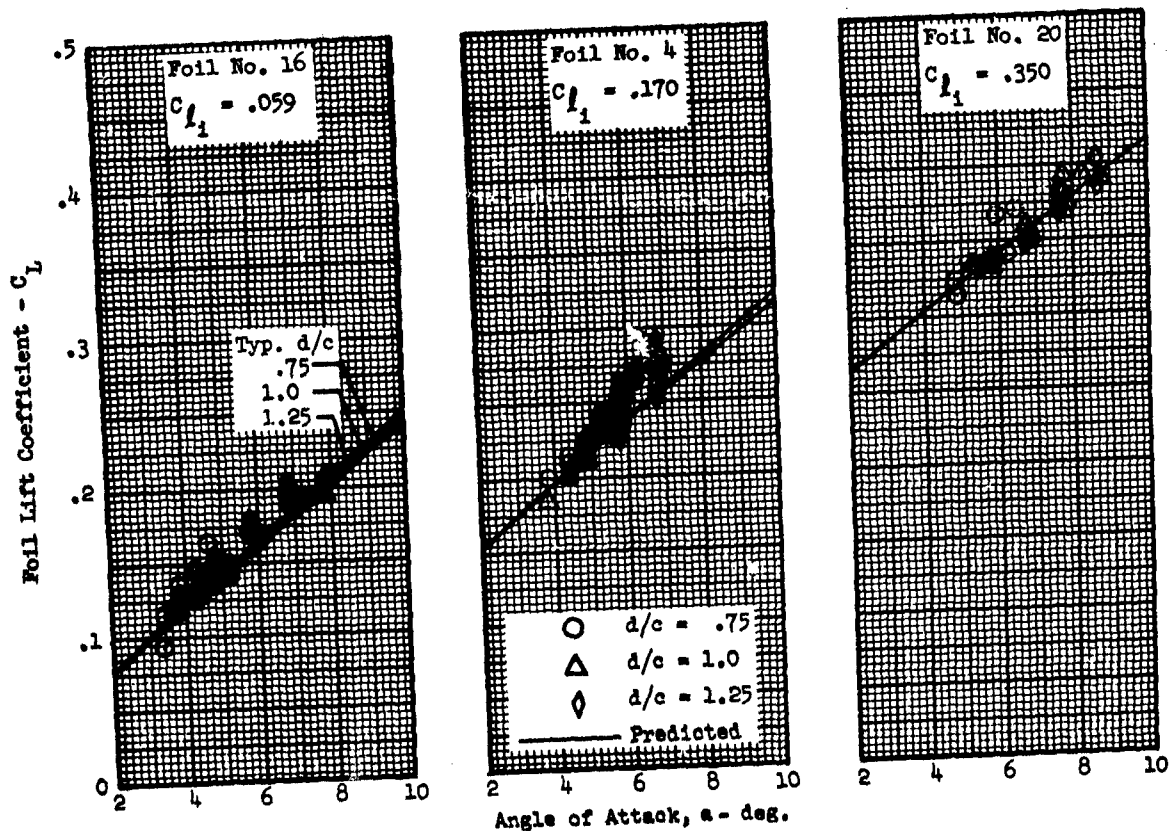


FIGURE 20 DRAG CORRELATION-ASPECT RATIO EFFECT

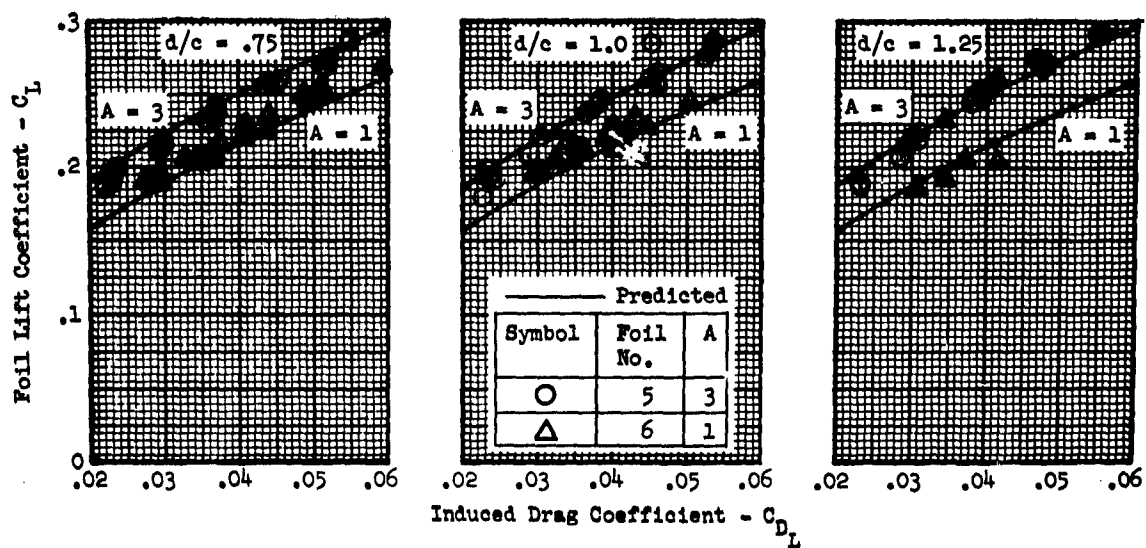
Parent Section - $C_{L1} = .170$ - $t/c = .131$
 $\Lambda = 0$
 $\lambda = 1.0$
 $\sigma = 0$


FIGURE 21 DF

A = 3

Symbol
◇
○
△
□
◇
◇

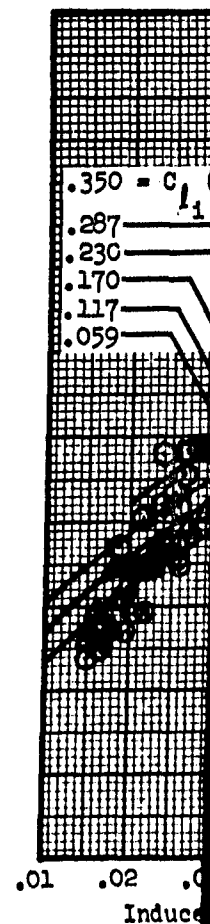
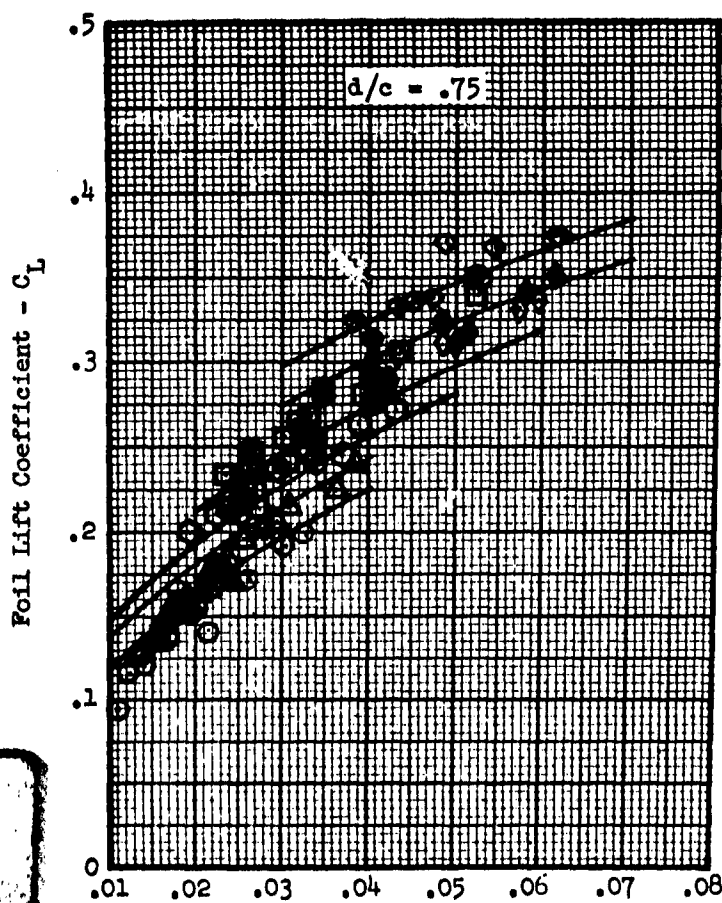


FIGURE 21 DRAG CORRELATION-CAMBER EFFECT

Parent Section

 $A = 3$ $\Lambda = 0$ $\lambda = .5$ $\sigma = 0$

Symbol	Foil No.	C_{l_1}	t/c
◇	4	.170	.131
○	16	.059	.071
△	17	.117	.103
□	18	.230	.158
◇	19	.287	.180
◇	20	.350	.203

Predicted

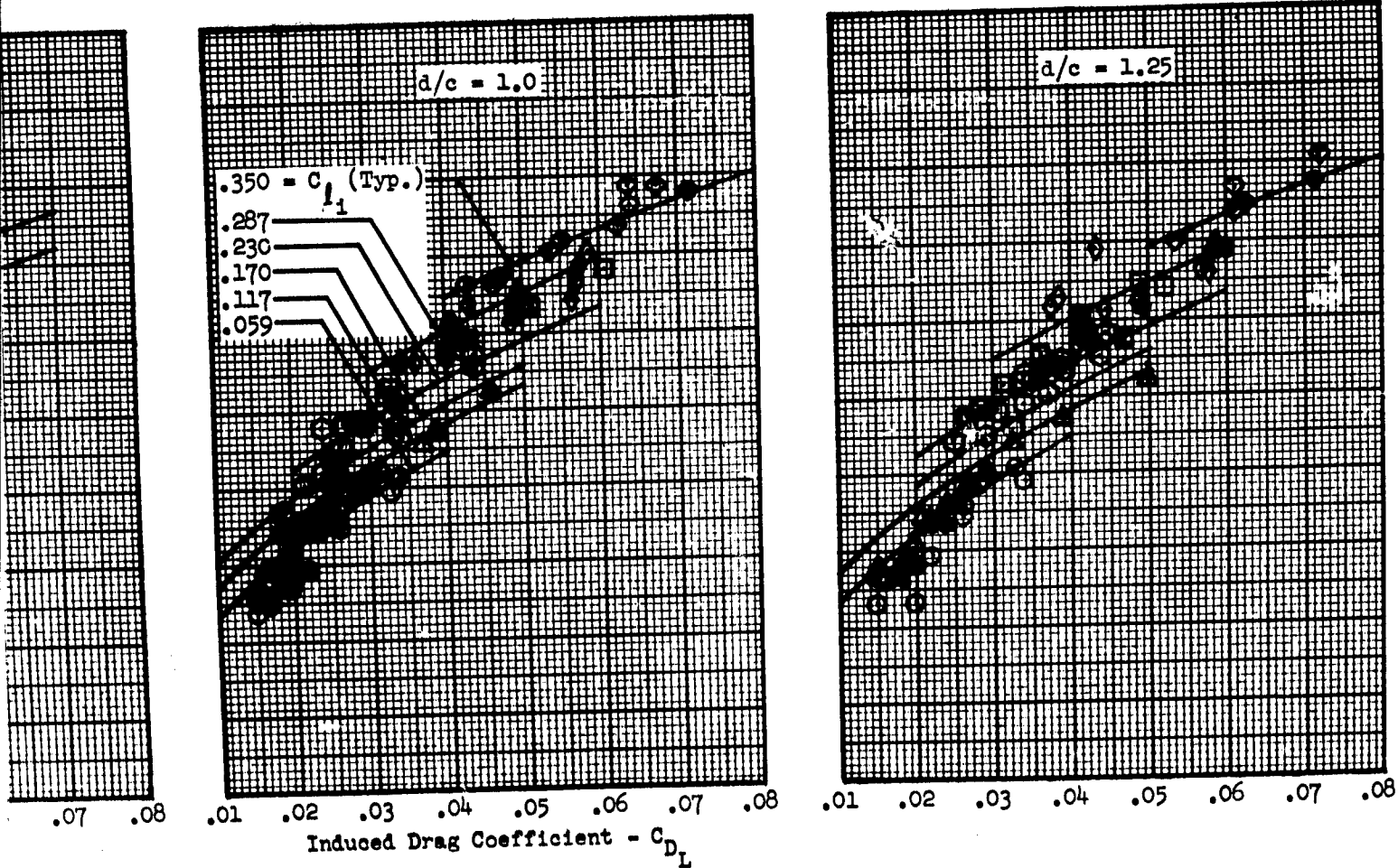


FIGURE 22 DRAG CORRELATION-TAPER RATIO EFFECT

Parent Section - $C_{D_i} = .170 - t/c = .131$

$A = 0$ $e = 0$ $A = 3.0$

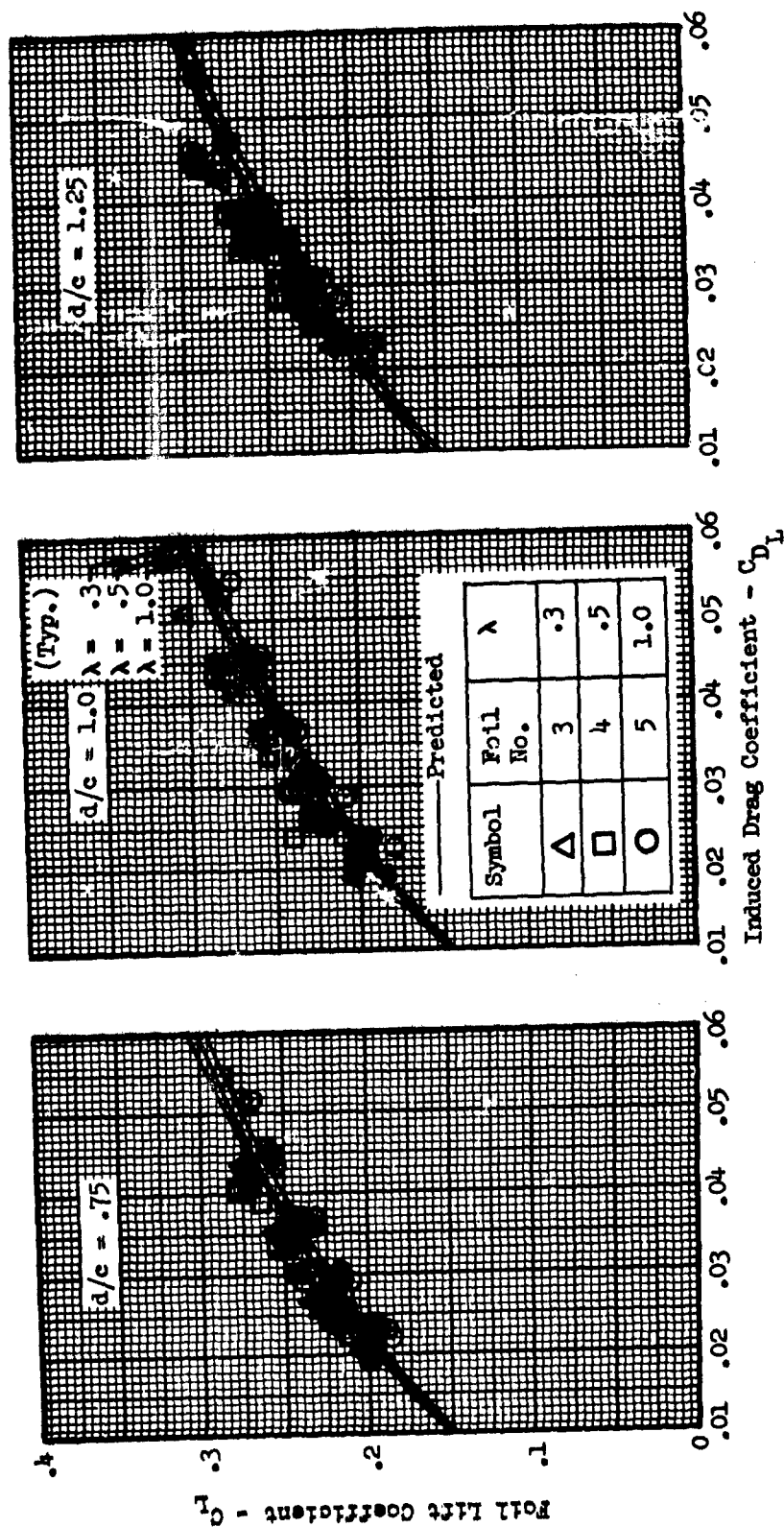


FIGURE 23 DRAG CORRELATION-SWEEP EFFECT
Parent Section - $C_{l_1} = .170$ - $t/c = .131$

$\lambda = .3$

$A = 3$

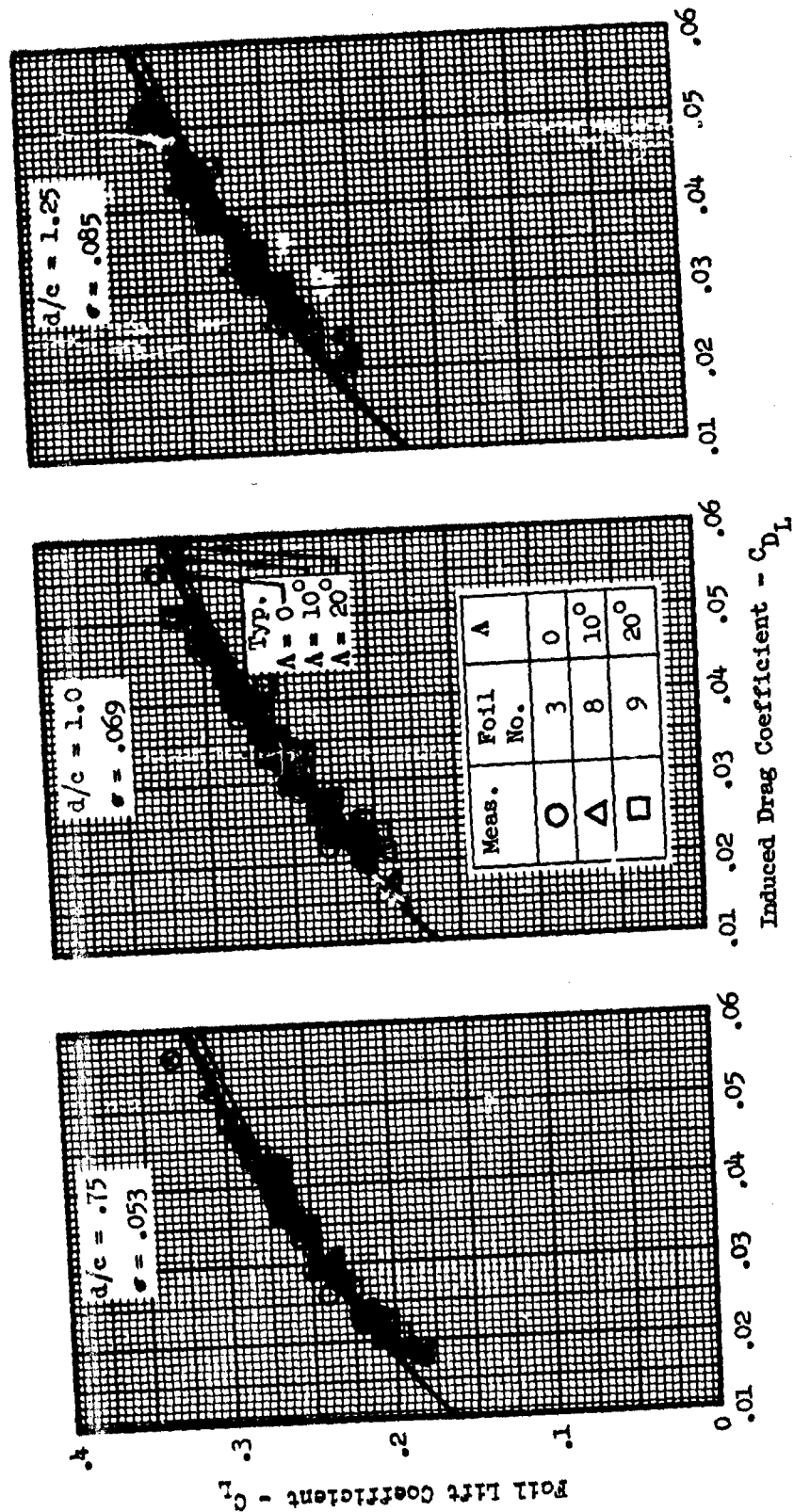


FIGURE 24 DRAG CORRELATION-SUBMERGENCE EFFECT

Parent Section

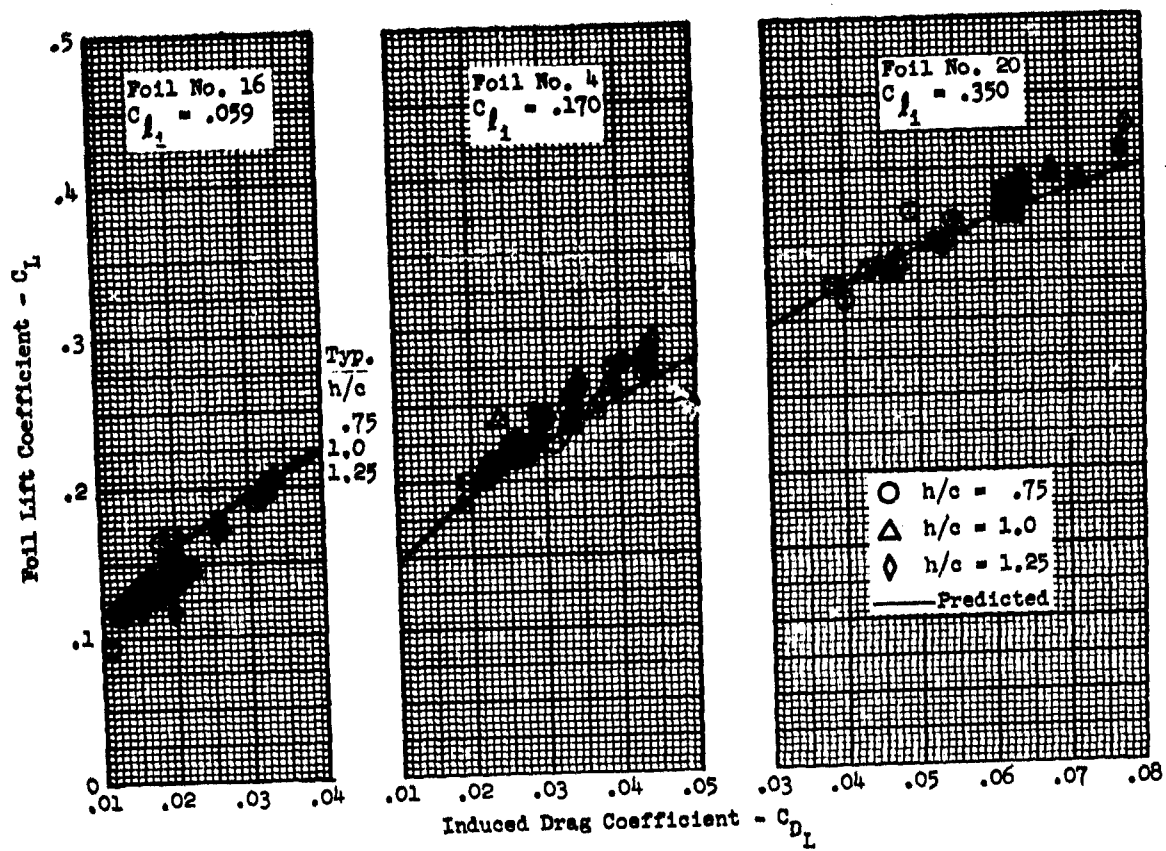
 $\lambda = 3$ $\lambda = 0$ $\lambda = .5$ $\sigma = 0$ 

FIGURE 25 DRAG CORRELATION VS. α -ASPECT RATIO EFFECT
Parent Section - $C_{Di} = .170 - t/c = .131$

$A = 0$ $\sigma = 0$ $\lambda = 1.0$

Symbol	Foil No.	A
O	5	3
Δ	6	1

— Predicted

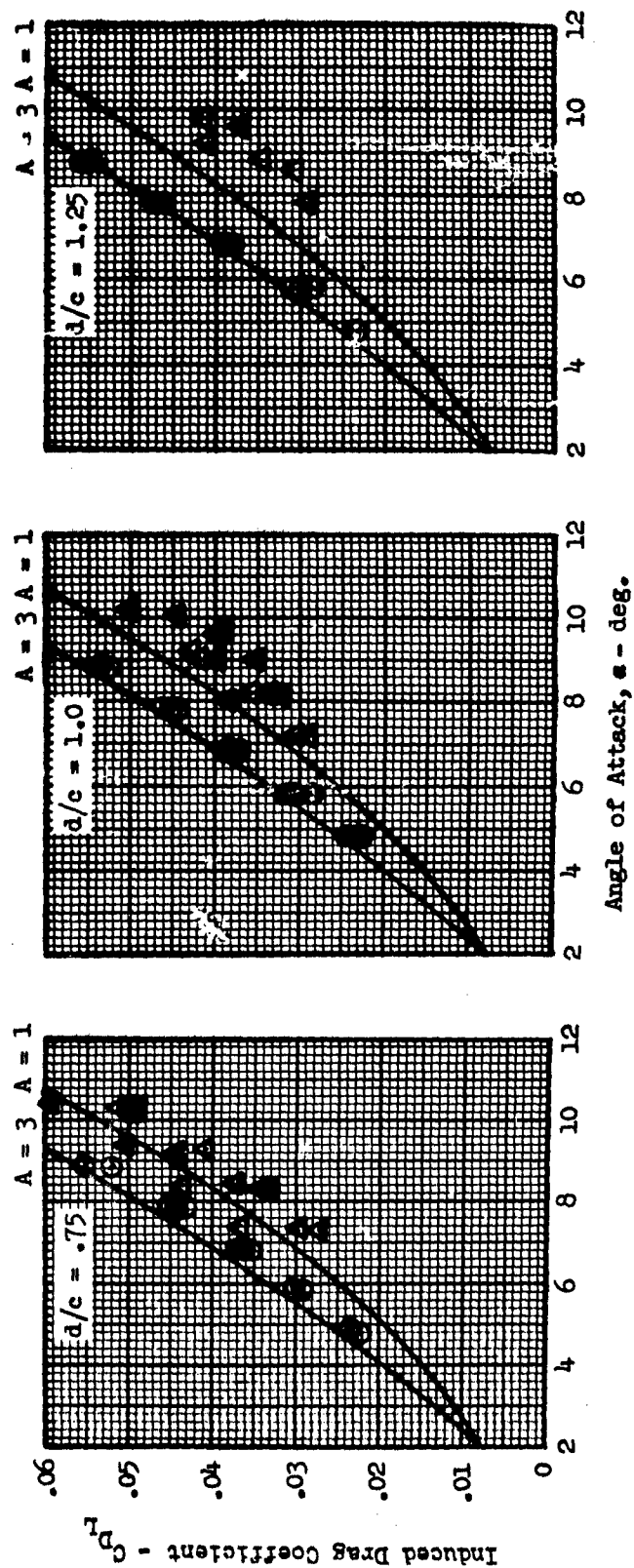


FIGURE 26 DRAG CORRELATION VS. α -CAMBER EFFECT

Parent Section

 $\Lambda = 3$ $\Lambda = 0$ $\lambda = .5$ $\sigma = 0$

Symbol	Foil No.	C_{l_1}	t/c
\square	4	.170	.131
\circ	16	.059	.071
\triangle	17	.117	.103
\square	18	.230	.158
\diamond	19	.287	.180
\diamond	20	.350	.203

— Predicted

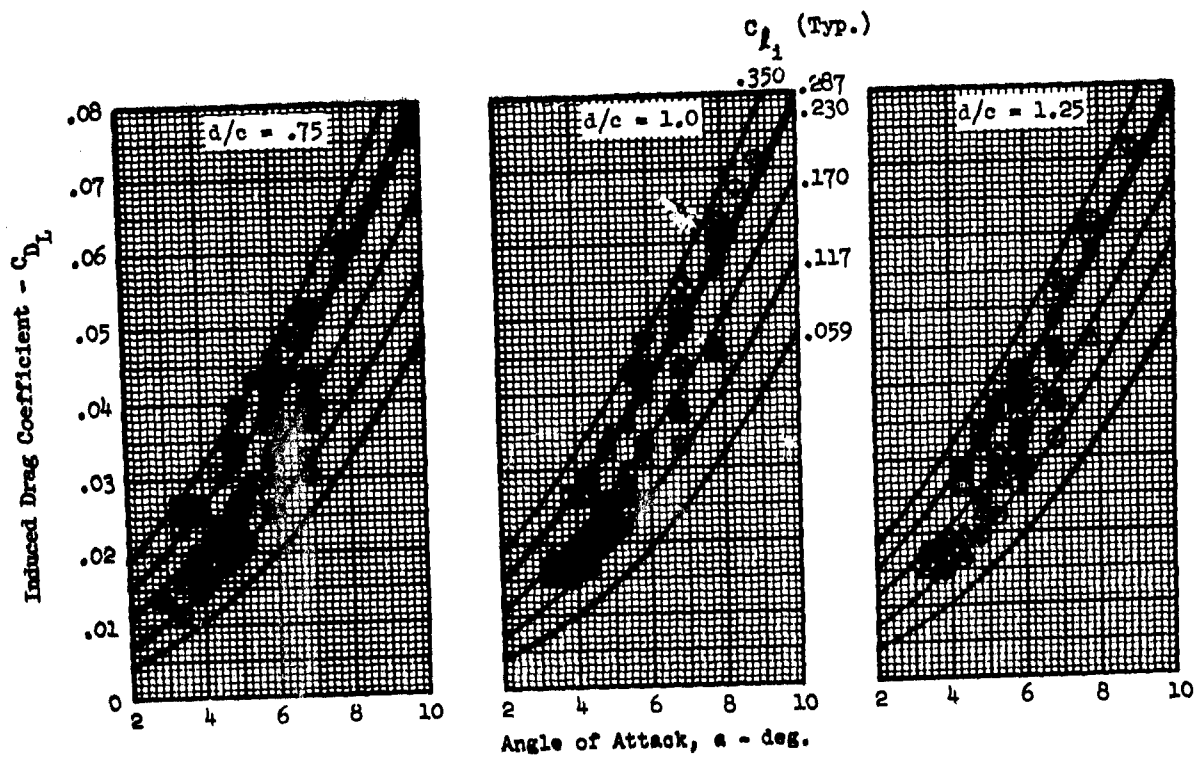


FIGURE 27 DRAG CORRELATION VS. α -FOIL No. 1Wedge - $C_{l1} = 0$ - $t/c = .118$ $A = 3$ $\Lambda = 0$ $\lambda = 1.0$

— Predicted

Symbol	V_K	$RN \times 10^{-6}$
○	40	.76
△	45	.85
□	50	.95
◇	60	1.14
◊	70	1.32
◻	80	~1.50

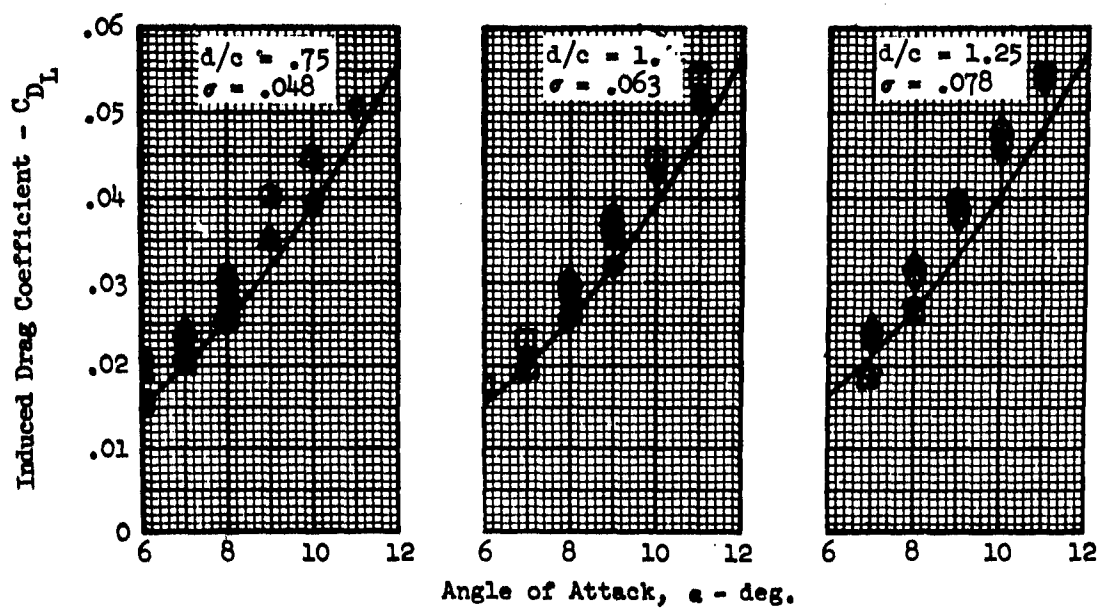
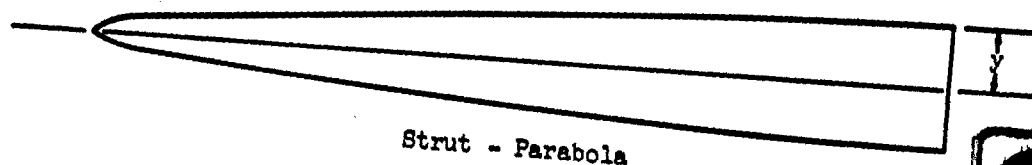
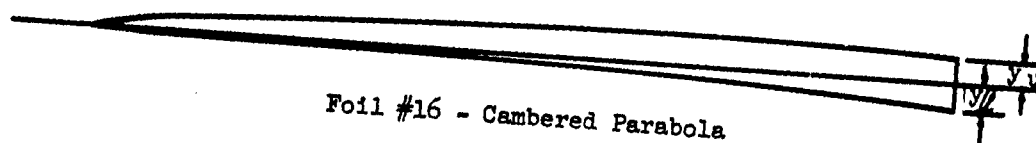
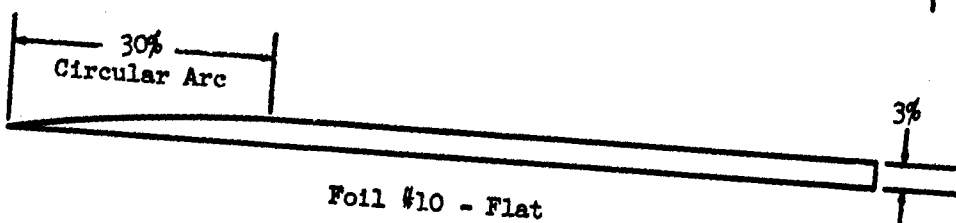
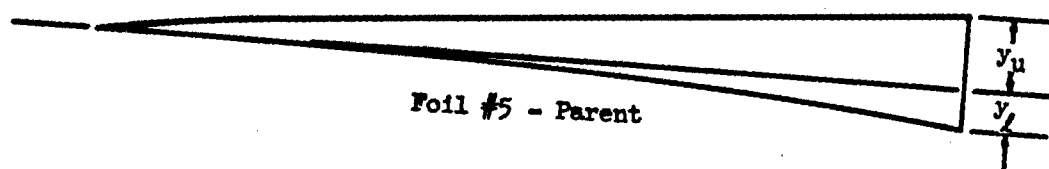
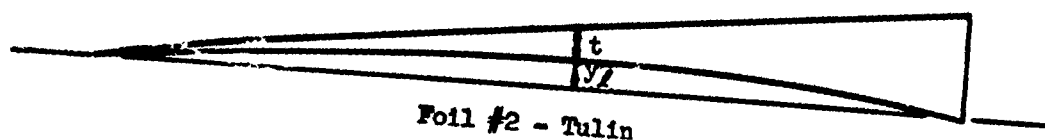
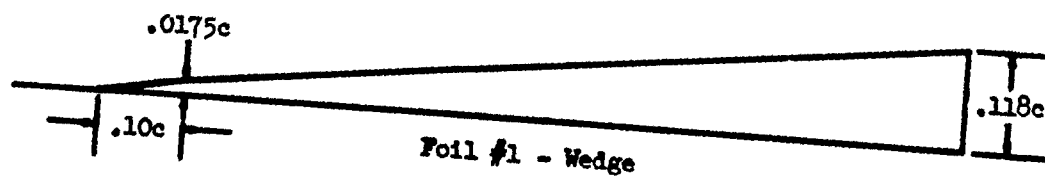


FIGURE 28
FOIL AND STRUT SECTIONS

$\frac{x}{c}$	Foil #2		Foil #5		Foil #16		Strut
	y_l/c	t/c	y_l/c	y_u/c	y_l/c	y_u/c	y/c
0	0	0	0	0	0	0	0
.0075	.00056	.00147	-	-	.00190	.00330	.00651
.0125	.00101	.00210	-	-	.00228	.00442	.00839
.025	-	-	.0003	.0053	.00288	.00660	.01186
.050	.00441	.00520	.0004	.0084	.00355	.00987	.01680
.075	-	-	.0007	.0115	.00398	.01246	.02054
.100	.00905	.00801	.0008	.0142	.00432	.01466	.02372
.200	.01759	.01272	.0017	.0194	.00546	.02138	.03354
.300	.02436	.01815	.0028	.0334	.00671	.02615	.04108
.400	.02893	.02505	.0045	.0419	.00826	.02968	.04744
.500	.03104	.03422	.0072	.0504	.01018	.03224	.05303
.550	.03112	.03950	.0090	.0544	.01130	.03320	.05560
.600	.03053	.04557	.0110	.0582	.01253	.03395	.05810
.700	.02726	.05944	.0161	.0659	.01538	.03482	.06275
.800	.02112	.07595	.0228	.0736	.01887	.03479	.06708
.900	.01207	.09521	.0314	.0812	.02329	.03363	.07115
.950	.00642	.10591	.0365	.0849	.02608	.03240	.07310
1.000	0	.11734	.0421	.0885	.03000	.03000	.07500





Strut	y/c
0	0
.00651	.00839
.01186	.01680
.02372	.02054
.03354	.04108
.04744	.05303
.05303	.05560
.05810	.06275
.06275	.06708
.06708	.07115
.07115	.07310
.07310	.07500
.07500	



UNCLASSIFIED

UNCLASSIFIED